An AFM Study of The Surface of A Polymer Film Bombarded by Low Energy Gaseous Ions

by Dixon D. He

A thesis

Submitted to the Faculty of Graduate Studies of the University of Manitoba in partial fulfillment of the requirement of the degree of

Master of Science

in

Mechanical Engineering

Winnipeg, Canada, 1997

THE UNIVERSITY OF MANITOBA

FACULTY OF GRADUATE STUDIES

*****

COPYRIGHT PERMISSION PAGE

AN AFM STUDY OF THE SURFACE OF A POLYMER FILM BOMBARDED BY LOW ENERGY GASEOUS IONS

by

DIXON D. HE

A Thesis/Practicum submitted to the Faculty of Graduate Studies of The University of Manitoba in partial fulfillment of the requirements of the degree

MASTER of SCIENCE

"There is plenty of room at the bottom."

Richard P. Feynman

Acknowledgments

First of all, I would like to thank Dr. M. N. Bassim, for guidance and assistance he generously provided through out the course of this research. I also benefit a lot from the graduate courses on materials engineering he has taught.

I would also like to thank Dr. D. J. Thomson of the Department of Electrical and Computer Engineering for letting me use his scanning force microscope. He is the person who first introduced me to the exciting world of Scanning Probe Microscopy by teaching the graduate course on STM and AFM.

Special thank is given to Jochonia Nxumalo for discussions on Atomic Force Microscopy. Thanks are also due to Dr. M. S. Mathur for providing the polyimide Kapton films, Doris Stevanovic of McMaster University for ion bombardment experiment and X. Y. Li for the latest version of TRIM code.

Finally I want to thank my parents and my wife for their love, encouragement and patience in the past years.

Abstract

This research studies the radiation damage on polymeric materials caused by accelerated ions. Gaseous ions are accelerated to different energies between 10 keV and 50 keV at fluences up to 10^{15} ions/cm^2 by 200 keV Whickham ion accelerator at room temperature. The 2×2 cm^2 polyimide Kapton films, with measured thickness of 62 micron, is bombarded by selected ions from an incident direction normal to target surface. The penetration depth of ions at this energy level is of a few microns which is much less than the thickness of the target, so the kinetic energy of the ion is completely deposited into the target to cause radiation damage.

The radiation damage results on the target is analyzed by contact mode atomic force microscopy (AFM) performed in ambient condition. Different types of surface topographic features are observed on ion bombarded Kapton. The depth of damage is measured and compared with the calculated result from TRIM program which is based on the ZBL (Ziegler, Biersack and Littmark) theory of stopping power and range. The

depth measurements and unique cross-section of the radiation-induced damage clearly support the proposed model for ion induced crater formation on a polymer surface.

List of Figures

List of Tables

Nomenclature

Kapton	Trade name of polypyromellitimide $(C_{22}H_{10}O_5N_2)_n$
μm	micron, 1 μm = 10^{-6} meter
Angstrom	1 angstrom = 10^{-10} meter
AFM	atomic force microscope or atomic force microscopy
TRIM	Transport Ion in Matter
keV	kilo-electron-volts
MeV	Mega-electron-volts
AECL	Atomic Energy of Canada Ltd.
NASA	National Aeronautics and Space Administration
SIMS	Secondary Ion Mass Spectroscopy
RBS	Rutherford Backscattering Spectroscopy
STM	Scanning Tunneling Microscopy
SPM	Scanning Probe Microscopy
SFM	Scanning Force Microscopy
nm	nanometer, 1 nm = 10^{-9} meter
FTIR	Fourier Transformed Infrared spectroscopy
$S_n(E)$	Nuclear stopping power

$S_e(E)$	Electronic stopping power
ε	reduced energy
Z_{eff}	effective charge
S_e(proton)	electronic stopping power of proton
GeV	Gig-electron-volts
Torr	unit of pressure
Gauss	unit of magnetic field
XPS	X-ray Photoelectron Spectroscopy
SPD	segment photodiode
PSPD	position-sensitive segment photodiode
PZT	piezotube
HOPG	highly oriented pyrolytic graphite

Table of Content

Chapter 1 Introduction

1.1 Prologue

For the past three decades, the radiation-induced property alterations on materials have attracted considerable interest in both academic research and industrial application. The irradiation effects which cause property changes to materials can be classified as irradiation-induced modification or radiation damage depending upon whether or not the property changes are desired. For example, as a property modification technique, ion beam technology has played a very important role in the semiconductor industry. On the other hand, a great amount of research has been put into studying the radiation damage to materials, from metal to polymer, in such environments as outer space and inside the nuclear reactor because of the serious concerns about safety and reliability.

The radiation-induced property change on materials can also be categorized in terms of the source of radiation and the energy of the incident particles. For studying irradiation-induced surface change in polymers, ions of energy below 50 keV are used. This falls into the category of low energy

ion radiation. At this energy level, most ions have a penetration depth of a few microns which is very important for surface properties. As one of its applications, the ion beam has be used to improve the surface property against wear and corrosion[1]. However most applications of the ion beam technique are in the semiconductor industry. Highly accelerated ions with energies of MeV have been used intensively to implant dopants into Si wafers and GaAs materials.

The main advantage of the ion beam technique is that all parameters associated with incident ions can be precisely controlled. These include energy, fluence, incident angle, mass and charge state of incident ions. Because of this feature, ion beams are not only utilized for material modification but also for simulating radiation damage to materials in special environments. NASA has conducted numerous experiments on radiation damages to its low orbit earth satellites caused by collision with energetic particles[2]. In Canada, scientists at AECL Chalk River Laboratory pointed out that the costly January 1994 failure of Canadian Telesat telecommunication satellite Anik E2 would have been prevented if its components had been tested in a simulated environment by their Tandem ion accelerator[3].

Several ion beam based analysis technologies have been developed to characterize the structures and compositions of materials. Among them Secondary Ion Mass Spectroscopy (SIMS) and Rutherford Backscattering Spectroscopy (RBS) have been widely used in surface study and proved to be successful on metals and semiconductors. Although these techniques can provide information of ion depth and chemical changes, they have a major drawback. Since both utilize an ion beam with energy from a few keV up to MeV[4,5], the impacts caused by incident ions sometimes may alter the surface and cause discrepancies on measurements. This effect may not be ignored especially in studying relatively soft materials such as polymers.

As a group of materials, polymers are relatively new compared to metals and alloys. However, for the past fifty years polymeric materials have dramatically changed the world of materials science and engineering as well as the life of ordinary people. The word polymer comes from the Greek words *poly* meaning "many" and *meres* meaning "parts". Although there are natural polymers such as natural rubber and silk, almost all polymers used today are synthetic polymers. Each polymer is a long chain molecule made by repeating a identical structure, called a *monomer,* to form big molecules with thousands of these repeat units. A typical synthetic

polymer sample contains chains with a wide distribution of chain lengths. Polymers can be classified by their processing characteristics or type of polymerization mechanism. More specific classification can be made on polymer structure. Instead of using the word polymer, the commercial materials, other than elastomers and fibers, that are derived from synthetic polymers are usually called plastics.

The polymer film used in this experiment belongs to a very important polymer family called polyimide. In general, polyimide has high-temperature and oxidation stability, good electrical-insulation properties and radiation resistance which have made them being widely used as electronic packing materials, cable insulators in nuclear reactors, matrix components of graphite composites for compressor valves in jet engine and insulating materials in spacecrafts[6]. The ion beam induced property change effects on polyimide have been studied in order to evaluate radiation damage in a simulated environment. Of many property changes in ion bombarded polyimide, surface topographic change has not been well studied until a couple of years ago because of the lack of an adequate tool for surface analysis. This situation has changed after the invention of atomic

force microscope (AFM) which is a important member of scanning probe microscope (SPM) family.

Since the Scanning Tunneling Microscopy (STM) was first developed by Binnig, Rohrer and Gerber at IBM Zurich Research Laboratory in the early 1980's [7], many types of scanning probe microscope (SPM) have been invented to study different properties of materials at atomic resolution. Among them, the atomic force microscope (AFM), referred as scanning force microscope (SFM) by some literature, is the most versatile one for surface study. Not only can it be operated on conductors, semiconductors and insulators, in air, vacuum and liquid, it can be used to study different types of surface properties. With these state-of-the-art surface analysis techniques in hand, scientists and engineers are now able to study the surface at atomic level as well as to build micromachines, motors and sensors, in nanometer (nm) scale. It is truly an exciting world for both researchers and industrial application developers. In this thesis, this surface analysis technology is used to study low energy ion bombarded polymeric materials.

1.2 The Origin of This Research

Unlike ion bombardment on semiconductors and metals, the study of ion beam induced damages on polymer is a relatively new area in terms of numbers and dates of research articles published. Besides limited numbers, most papers published before the 1990's are focused on the depth profile and range of ions in polymers which are important to ion implantation technology. The surface topographic study on ion bombarded polymeric materials began in the late 1980's after scanning force microscopy was developed. So far it is still a developing area where both experimental and theoretical researches are quite active.

I first got into this study in 1993 when I was working as a research assistant at the accelerator center of the University of Manitoba. At that time our group was interested in studying proton induced radiation damage on Kapton film, which has been used as an insulator in nuclear reactors, under a controlled environment. To simulate this process, Kapton film and mica have been bombarded by hydrogen and deuterium ions accelerated by 120 keV Narodny linear accelerator at different energies.

Since the Narodny ion accelerator was designed and built in the early 1970's, the ion beam is focused as a circular spot on the target surface rather than scanned as in most late model ion accelerators. Beside frequently occurring problems with cooling and vacuum systems, the worst part of Narodny was it did not even have a mass analysis system until one was installed and calibrated in the summer of 1993. After we managed to fix all these problems, the experiment of deuterium ion bombardment on Kapton was conducted. On the ion bombarded Kapton film, a darkened circular spot was clearly visible. This "darken" effect is the most common effect on ion bombarded polymers. It indicates the degradation of polymer which is generally caused by chain scission induced formation of carbon islands and release of free radicals[8a, b].

The traditional surface analysis technologies such as Raman Spectroscopy and Fourier Transformed Infrared Spectroscopy (FTIR) have been used in previous research. All those technologies have the drawback of producing averaged information of surface rather than resolving spatial information locally. So it was decided to utilize the atomic force microscope (AFM) to study the ion bombarded polymer surface. After taking a graduate course on STM and AFM from Dr. D. J. Thomson at the Department of

Electrical and Computer Engineering, I was able to take surface images by using STM and AFM. In the summer of 1994, many images were taken from ion bombarded Kapton film and ion beam induced crater formation with unique cross-section profile was first observed. Two years later, in 1996, a paper based on this research was accepted and published by Materials Science and Engineering (B) [9].

While I was going to extend this research by investigating the radiation effects on Kapton caused by different ions at different energies and fluences, the project was suspended for various reasons. It was not resumed until the fall of 1996 when Dr. M. N. Bassim shown his interests in this research and decided to support it. Since then more ion bombardment experiments have been conducted on the 200 keV Whickham ion accelerator at McMaster University. Kapton films were bombarded by Deuterium, Helium, Nitrogen and Argon ions at energy from 10 keV to 50 keV and fluence from 10^{13} to 10^{15} ions/cm^2. Hundreds of surface images have been taken by AFM. More features have been observed and a model is proposed in order to explain crater formation on Kapton surfaces.

1.3 The Aim and Scope

The aim of this research is to study the ion induced radiation damages on polyimide Kapton surface. To achieve this goal, surface images have been taken from ion bombarded surface and the depths of surface damages are measured by using atomic force microscope (AFM). Theoretical calculations of depth and range are carried out by using TRIM program. The experimental and calculated results are compared in order to evaluate results and discrepancies. A model based on diffusion and trapping is proposed to explain the mechanism of forming craters on the surface, and the relative large discrepancies between experimental and calculated values.

The theory of diffusion and trapping in ion bombarded polymer has not yet been established. Therefore, numerical calculation of these processes is not available in this thesis. Due to limited resources, time and equipment, radiation induced chemical changes in ion bombarded polyimide Kapton are not in the scope of this research. Fortunately, previous researches of chemical changes in ion bombarded polymers provide considerable information on this issue.

1.4 Organization of This Thesis

The thesis is organized in a formal way which is adopted by most of scientists and engineers for their scientific writings. In chapter two, the physics of stopping an energetic ion in matter is briefly introduced. The focus is on the basic mechanism, definitions and procedures rather than explaining quantum mechanics. As a major tool for theoretically studying the interactions between incident ions and target atoms, the simulation and calculation program TRIM (Transport Ions in Matter), which is developed based on the ZBL (Ziegler, Biersack and Littmark) theory, is described.

The experimental techniques are described in Chapter three. The chemical structure and physical properties of Kapton are presented in "specimen preparation". Then, the ion beam technology and atomic force microscopy are explained in the second and third section respectively.

The results are shown and discussed in Chapter four. Surface topographic images and measured depth are compared with the results from previous works and theoretical calculations respectively. The cross-section profile of ion induced damage on surface are shown in the last section of

Chapter four. The formation of craters is also discussed in this part. A model of crater formation on a polymer surface is introduced.

In the last Chapter, conclusions are made from this research and clearly summarized. Some recommendations for future researches in this area are also presented.

Chapter 2 Theory

When energetic ions approach and enter the surface of target, they interact with atoms or molecules in the solid, lose their kinetic energy, and eventually come to a stop where the incident ions only maintain their thermal energy. This process is called the stopping of ions in a solid. It took more than a half century for physicists to understand the mechanism of the interactions between energetic ions and the atoms in a solid.

The research on stopping of energetic ions in matter started in early 1900's when scientists were trying to determine atomic structure. In 1913, Niels Bohr, who was working as a postdoctoral scientist at Rutherford's Manchester Laboratory, published a paper of his ideas on a model of the atom which was based on the study of the stopping of charged particles by a solid[10]. In the paper, He concluded that the energy loss of ions passing through matter could be divided into two components. The first part is the energy loss to target nuclei and the second part is energy loss to target electrons. He also predicted that the first part would be much less than the second part when the energy of incident ions is sufficiently high. Although Bohr's study of energy loss process was limited by lack of information of

the charge state of ions inside matter, his study formed the foundation of the theory of stopping ions in matter.

A major advance in understanding stopping power came twenty years later when Bethe and Bloch restated the problem from the perspective of Quantum Mechanics and derived the Born approximation of the fundamental equations for stopping of fast particle in a quantified electron plasma[11a, b]. In the late 1930's, scientists studied the problem of how to treat the interaction of a partially stripped heavy ion. "Effective charge" was introduced. Bohr worked out the expression of effective charge and screening distance between two colliding atoms which limits the energy transfer between nuclei[12a, b].

From the 1950's to 60's Lindhard concentrated on non-relativistic particle interacting with a free-electron gas and provided a full general treatment based on a few assumptions[13]. His work is widely cited in literature as it formed part of the first unified theory. Many calculations have been carried out using Lindhard theory and many tables have been produced based on these calculations[14a, b]. However, the difference between measured range and calculated range was sometimes of a factor of two.

During the 1960's and 70's the major advance came by applies numerical methods to tradition theoretical approaches. In 1970's and 80's Ziegler[15] and Biersack[16] made more contributions to stopping theory and range algorithm respectively. Based on their work, a computer program called TRIM (Transporting Ions in Matter) was developed to simulate the stopping process of ions in matter and calculate the depth profiles and range[17].

Since then the accuracy of TRIM calculation has been continuously improved. Now the discrepancy in stopping power calculation is less than 2% for high energy ions and around 10% for low energy ions[18]. However, most of these results were obtained from ion bombarded metals and semiconductors. Many recent studies on ion bombarded polymers show that discrepancy varies from around 20% to 40%[19a, b]. A major limitation of these calculations is that the thermal effects and radiation-induced diffusions are not included in the above theory. The mechanism of thermal and diffusion effects is not only interesting to scientists but also to engineers because it may result better control of ion distributions in solid. Although many models are suggested in order to explain diffusion related phenomenon, so far a complete theory is still not available. In the past few

years, more and more research interests have switched into this area. Among the materials studied, polymer has drawn special attentions because their potential applications in electronic and fiber-optic devices. As an attempt to solve this problem, a model based on this research is proposed in chapter four.

2.1 Stopping Power and Range

When an ion enters the target surface, the incident ion loses its kinetic energy to atoms in the target. The energy transfer between a moving and a stationary charged particle depends on the mass and the charge of the two particles, and the initial velocity of the incident particle. While the incident particle approaches, the interactions between two particles cause velocity change on moving particle while the stationary particle recoils and absorbs energy as shown in Figure 1.1. The final velocity and trajectories of both particles can be found from conservation of momentum and energy of the system. Numerical methods have been developed to evaluate the more complex collision of atoms with shell effects, and the absorption of energy into the Pauli promotion of the electrons. Assumptions have been made in order to simplify this problem. Firstly, no evaluation is made for thermal effects in the solid especially redistribution of atoms or ions by thermal or defects induced diffusion. Secondly, the energy loss of ion can be separated into two components, namely nuclear stopping power and electronic stopping power. Thirdly, the target is considered to be amorphous with atoms at random locations.

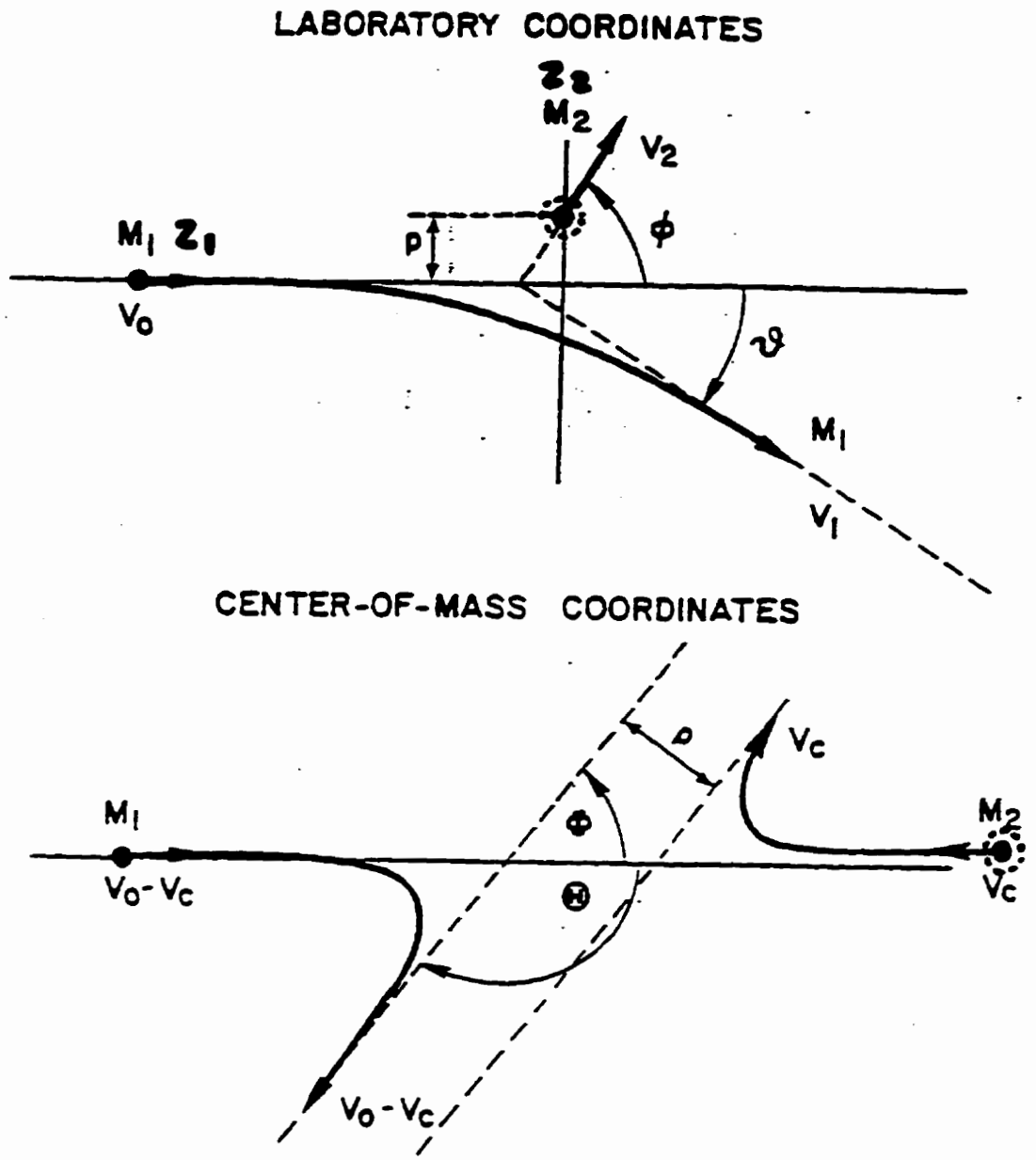

Figure 1.1 The collision of an incident ion with a target atom

It is noteworthy that separation of the energy loss of the ion into two separated components ignores the possible correlation between elastic nuclear collision and inelastic losses to electronic excitation. It seems that this correlation probably is not significant when many collisions are averaged.

2.1.1 Nuclear Stopping Power

The nuclear stopping power, $S_n(E)$, is the elastic energy transferred to the stationary atom which can be treated as the kinetic scattering of two heavy screened particles. The energy lost by ion per path length is dE/dx which is related to nuclear stopping power by

$$dE/dx = NS_n(E)$$

where N is the atomic density of target.

For practical calculations, the universal nuclear stopping power is

$$S_n(E) = \frac{8.462\times10^{-15}\, Z_1 Z_2 M_1 S_n(\varepsilon)}{(M_1+M_2)(Z_1^{0.23}+Z_2^{0.23})} \text{ eV (atom/cm}^2\text{)}$$

with the reduced energy, ε, being calculated as

$$\varepsilon = \frac{32.53\, M_2 E_o}{Z_1 Z_2 (M_1+M_2)(Z_1^{0.23}+Z_2^{0.23})}$$

and the reduced nuclear stopping being calculated as:

For $\varepsilon \leq 30$:

$$S_n(\varepsilon) = \frac{\ln(1 + 1.1383\,\varepsilon)}{2[\varepsilon + 0.01321\,\varepsilon^{0.21226} + 0.19593\,\varepsilon^{0.5}]}$$

For $\varepsilon > 30$:

$$S_n(\varepsilon) = \frac{\ln(\varepsilon)}{2\varepsilon}$$

2.1.2 Electronic Stopping Power

The electronic stopping power is the inelastic energy transferred to the electrons of a stationary atom by electronic excitation. Compared to nuclear stopping power, the physics of electronic stopping power is much more complicated. It was originally treated as classical energy transferred by a moving charged particle to a free electron[20]. By bringing quantum mechanics into this problem, the Bethe-Bloch theory considers a particle interacting with an isolated atom of harmonic oscillators. This approach solved the charged particle energy loss problem quantum mechanically in the first Born approximation. However, this theory shall be only used for high energy (>10 MeV/amu) relativistic stopping[21].

The next major step in electronic stopping theory came from the consideration of the target as a collection of interacting electrons, i.e. a plasma, and to consider the energy loss to collective effects such as dynamic polarization, and to plasmons. After making some assumptions, Lindhard treated this problem by presenting a generalized method of an electron gas responding to a perturbation of a charged particle[22]. It naturally includes the polarization of the electrons and the resultant charge screening and plasma density fluctuations. After using the local density approximation it can be directly applied to any target and the effects of chemical bonding or crystal structure on stopping power are simply evaluated. The calculation of electronic stopping power is mainly based on the scaling of the ions under consideration to the well-known proton stopping power.

$$S_e(E)=Z_{eff}^2 S_e(\text{proton})$$

where S_e is electronic stopping power of proton and Z_{eff} is effective charge of the incident ions. If Z_1 is the atomic number of the ion, v is the ion velocity and v_o is the Bohr velocity (~ 2.2×10^8 cm/sec), then Z_{eff} can be calculated by $Z_{eff}=Z_1^{1/3}\, v/v_o$. The practical calculation of electronic stopping power can be carried out as following:

(1) For hydrogen ions, a fitted function to obtain hydrogen stopping power in each element can be directly used.

(2) For helium ions, the equivalent hydrogen stopping is multiplied by the helium effective charge at that velocity.

(3) For heavy ions, the proton stopping power is scaled based on Brandt-Kitagawa theory[23].

(4) For very low velocity ions (<30keV/amu), the velocity proportional energy loss theory is used.

2.1.3 Range of Ions

To determine ion range and damage distribution as well as angular and energy distribution of ions, the Monte Carlo method which simulates slowing down and scattering of energetic ions in an amorphous target is applied. The Monte Carlo method has a number of distinct advantages over analytical formulations based on transport theory. It allows more rigorous treatment of elastic scattering, explicit consideration of surfaces and interfaces, and easy determination of energy and angular distributions. The major limitation of this method is that there is often a conflict between available computer time and statistical accuracy. To increase the computer

efficiency while still maintaining proper accuracy, the distance between collisions is suitably extended and an analytic formula is applied for determining nuclear scattering angles.

The Monte Carlo method follows a large number of individual "histories" of ions and atoms in the target. Each history begins with a particle with given initial energy, position and velocity. The particle is assumed to change direction as a result of binary nuclear collisions and moves in straight free-paths between collisions. Its energy is reduced as nuclear and electronic energy losses which are assumed to be independent as mentioned before. Therefore, the particle loses its energy in discrete amounts by nuclear collisions and continuously through electronic interactions as described in the previous section. A history is terminated when the kinetic energy drops bellow a certain value or the particle is outside the target which is assumed to be amorphous. Then, the range is calculated from the history. Relativistic effects and nuclear reactions are not considered in this approach.

2.2 TRIM Program

Based on the theoretical treatment of ion-atom collisions, a computer program TRIM (Transport Ions in Matter) has been developed to calculate the transport of energetic ions (10 eV--2 GeV) into matter[24]. By using a statistical algorithm, Monte Carlo method, the range is calculated from the collision results over the ion trajectory. All the target atom cascades in matter are also followed in detail as shown in Figure 2.1.

During the collisions, the ions and atoms have a screened Coulomb collision which includes exchange and correlate interactions between the overlapping electron shells. The long range interaction between ions and atoms results on electron excitation within the target. These are described by including a description of the target's collective electronic structure and inter-atomic bond structure when setting up calculation.

The charge state of the ion within the target is described using the concept of effective charge which includes a velocity dependent charge state and long range screening due to the collective electron sea of the target. The updated TRIM-95 program is able to calculate all kinetic phenomena associated with the ion energy loss such as target damage,

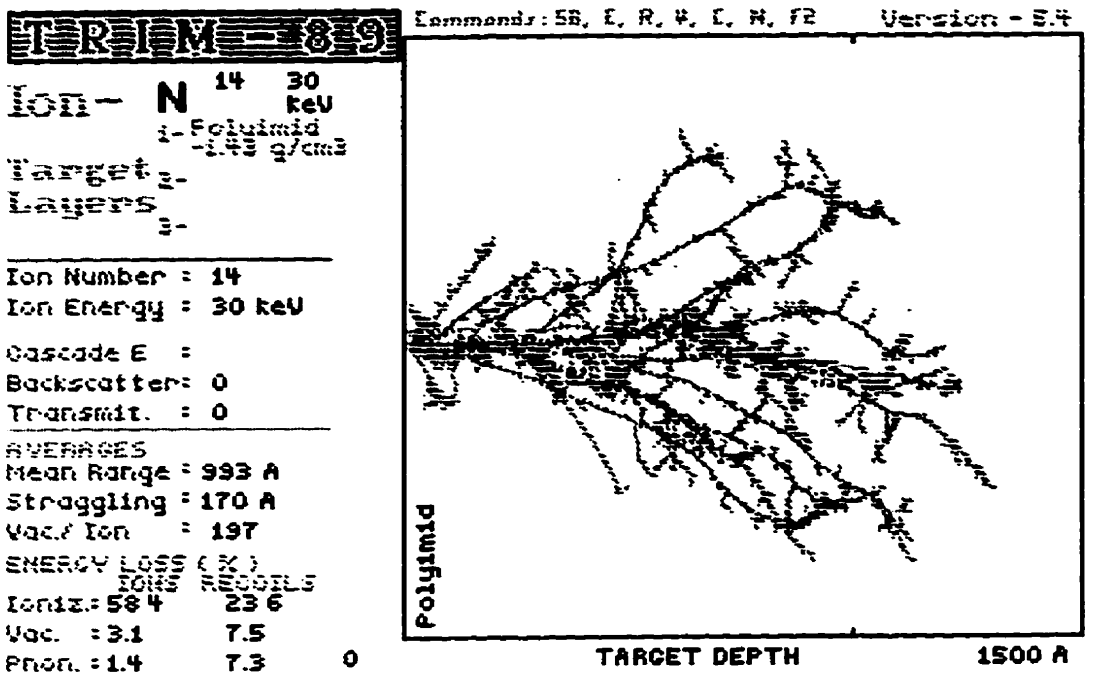

Figure 2.1 TRIM simulation of ion trajectory and atom cascades

ionization, sputtering and phonon production. Its main features are listed as following:

(i) accepts targets made up to three layers of different materials

(ii) calculates depth profile

(iii) calculates energy loss profile

(iv) calculates ionization profile

(v) includes atom cascade and vacancy generation

(vi) simulates 3D distribution of ions

The TRIM program works on PC 386 and 486 computers with a color monitor, a co-processor and about 530 K of free RAM. It works with version 2.+ of OS/2 operating system which includes Microsoft DOS as a full-screen sub-session. Although not running on Windows, it has a user friendly interface which enables the user to select all the parameters on the screen. To set up a calculation, the user only needs to follow the on-screen procedure, step by step, to choose parameters such as ion mass and energy, type and thickness of the target, number of ions to be followed and so on. For a polymer target, the TRIM program provides a target table which includes Kapton for user to select from. After the parameters being selected,

the TRIM program starts to calculate the stopping powers. Since there are carbon, hydrogen, oxygen and nitrogen atoms in Kapton, stopping power is calculated for each atom separately. These calculations take only a few seconds to complete on a 486DX 66 MHz PC with 16 MB of RAM.

By using the Monte Carlo method, the simulation can be conducted for either quick calculation of damage or detailed calculation with full damage cascades. The first option calculates the final ion distribution, ionization energy loss by ion, energy transferred to recoil atoms. Shown in Figure 2.2 and 2.3 are the ion induced target vacancy distribution and ion range calculated by TRIM program. In addition to this, the second option follows every atom recoil until its energy drops below the lowest energy for an atom displacement. Thus, all collision damages to the target are analyzed. It takes several minutes to hours to complete a simulation mainly depends on the number of ions to be calculated. The results of the calculations are presented by both tables and curves.

Although the latest version I have is TRIM-95 which has much a better on-screen display than TRIM-89, I still use TRIM-89 for most of calculations simply because TRIM-95 has never worked as reliably as

TRIM-89 does. Besides, I have not been able to print from TRIM-95 to take advantage of its high quality display feature.

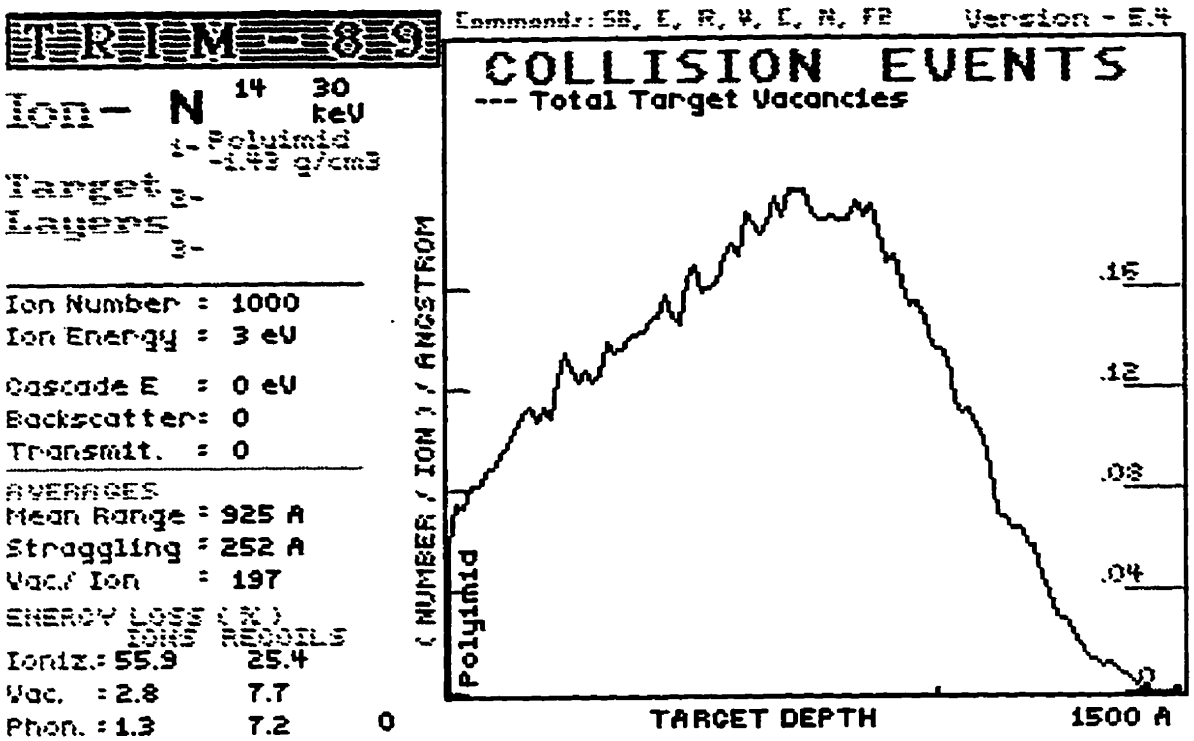

Figure 2.3 Defect distribution for 30 keV N^+ ions calculated by TRIM

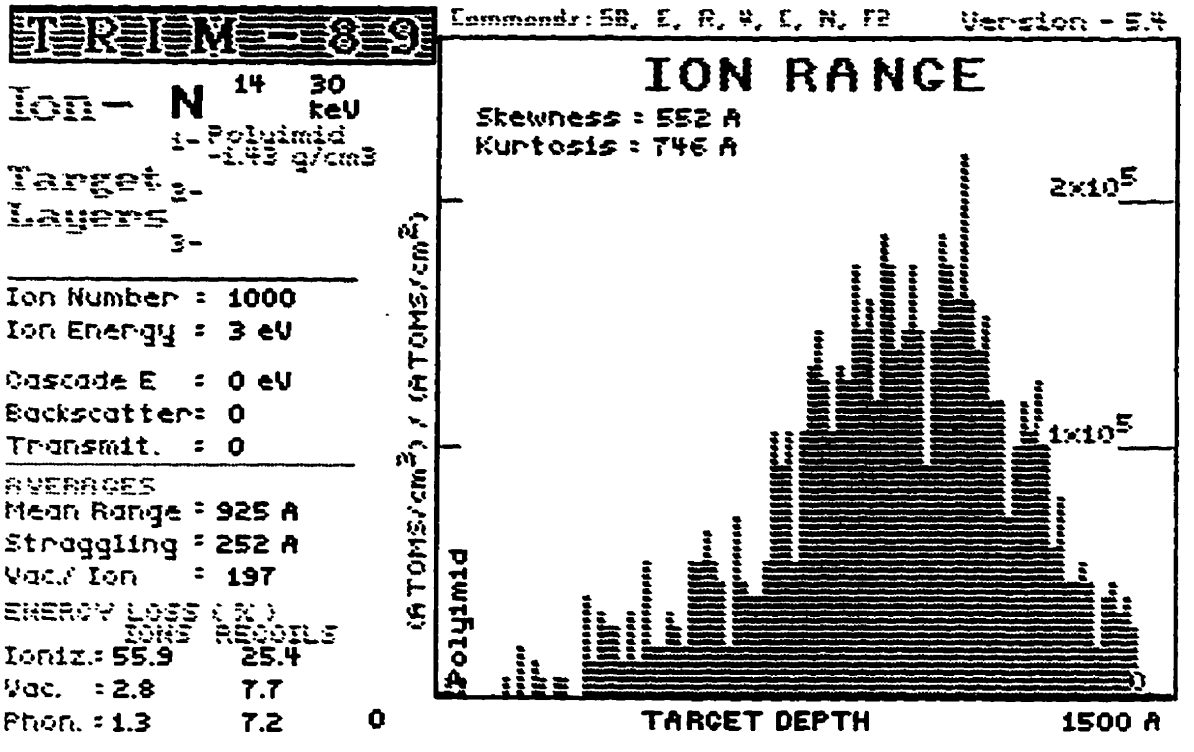

Figure 2.3 Ion range for 30 keV N^+ ions calculated by TRIM

Chapter 3 Experimental Procedures

3.1 Specimen Preparation

The polymeric material used in this experiment is polyimide Kapton. Polyimides represent an important group of high-temperature, solvent-resistant polymers which have a small but steady commercial market in the aerospace and electronics industry and for biomedical applications. Polyimides are formed by a two-stage process. The first step involves the polycondensation of an aromatic dianhydride and aromatic diamine to form an intermediate poly(amic acid). Then dehydration of the poly(amic acid) at elevated temperatures yields the polyimide (PI) structure. Unlike the intermediate poly(amid acid), the fully imidized polyimide is insoluble, infusible, and has high-temperature, oxidative stability, good electrical-insulation properties and radiation resistance.

Kapton is the trade name of polypyromellitimide $(C_{22}H_{10}O_5N_2)_n$ which is a DuPont product. It is obtained by the condensation polymerization of pyromellitic anhydride and 4,4-diamino diphenyl ether. During these "imidize" process, possible structure weakness of the fully

imidized product may be caused by void formation due to water release in the imidize process. The chemical structure of Kapton is shown in Figure 3.1. It is noteworthy that the benzene rings play a important role in its radiation resistance. As one of the most widely used polyimide, Kapton has been frequently used as an insulator in nuclear reactors and thermal blankets in spacecraft[25].

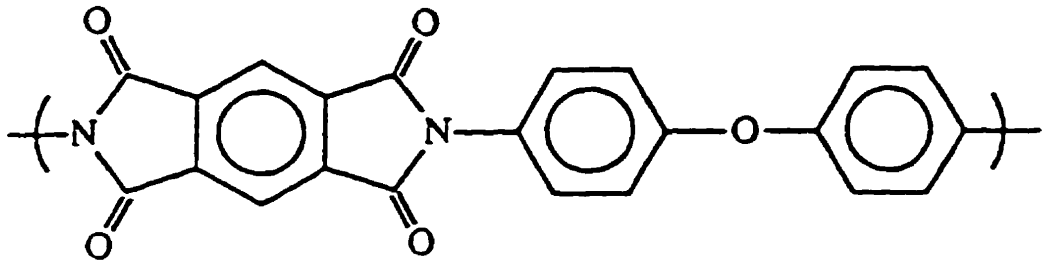

Figure 3.1 The chemical structure of polyimide Kapton

The thickness of Kapton film used in my experiment is 62 μm. It is a amber color polyimide with a density of 1.43 g/cm^3 and glass transition temperature (T_g) of 385 °C. At room temperature, the tensile strength and elongation of Kapton at fracture are 172 MPa and 70% respectively[6]. The surface smoothness of this film is about the same as most glass surfaces in term of reflection. Its properties are shown in Table 3.1 and Table 3.2. Before mounted onto target holder, Kapton film is cleaned and cut into 2 ×

2 cm^2 size. A thin layer of silver paste is applied to the side which contacts the target holder made of copper. After ion bombardment, specimens were put into a sealed container and stored in a dark place at room temperature.

Table 3.1 Target composition and core stopping (eV)

Atom Name	Atom Number	Relative Abundance	Core Stopping (eV)
H	1	10.000	0.000
C	6	22.000	6.145
N	7	2.000	5.859
O	8	5.000	5.446

The time interval between ion bombardment and surface study by AFM varies from a few days to six months. In order to remove contamination on the surface, specimens were treated by a mild NaOH solution for less than thirty seconds than washed by distilled water. The water remaining on the surface is absorbed by Kimwipes EX-L extra low-lint wipers before completely dried out in air.

Table 3.2 Target bonds and their stopping (eV)

Target bond type (Kapton)	Bond number per molecule	Bond stopping (eV)
(H-C)	10	7.244
(C-C)	13	3.938
(C=C)	9	9.790
(C-N)	6	5.080
(C-O)	2	6.168
(C=O)	4	13.926

3.2 Ion Bombardment

The ion bombardment experiment was originally conducted on a Narodny ion accelerator at the University of Manitoba. The Kapton film was bombarded by 30 keV Deuterium ions at a fluence of 10^{12} ions/cm^2. After ion bombardment the irradiated surface has been scanned by AFM and ion damage of circular shape were spotted[9].

Most of the recent experiments have been done at the Department of Engineering Physics of McMaster University. Shown in Figure 3.2, the ion accelerator at McMaster University is a 200 keV heavy ion accelerator designed and manufactured by Whickham Engineering Ltd. of England in the early 1980's. It is a general purpose instrument which is capable to produce high intense beam current with a high degree of flexibility and reliability.

As most ion accelerators, this 200 keV Whickham linear ion accelerator utilized a static electrical field to accelerate charged particles. It consists of an ion source chamber, analyzing magnet, beam monitor chamber, post acceleration column and target chamber as shown in Figure 3.3* . All these components are evacuated to a vacuum of pressures less than

* Courtesy of Whickham Engineering Ltd., England

Figure 3.2 The 200 keV Whickham ion accelerator

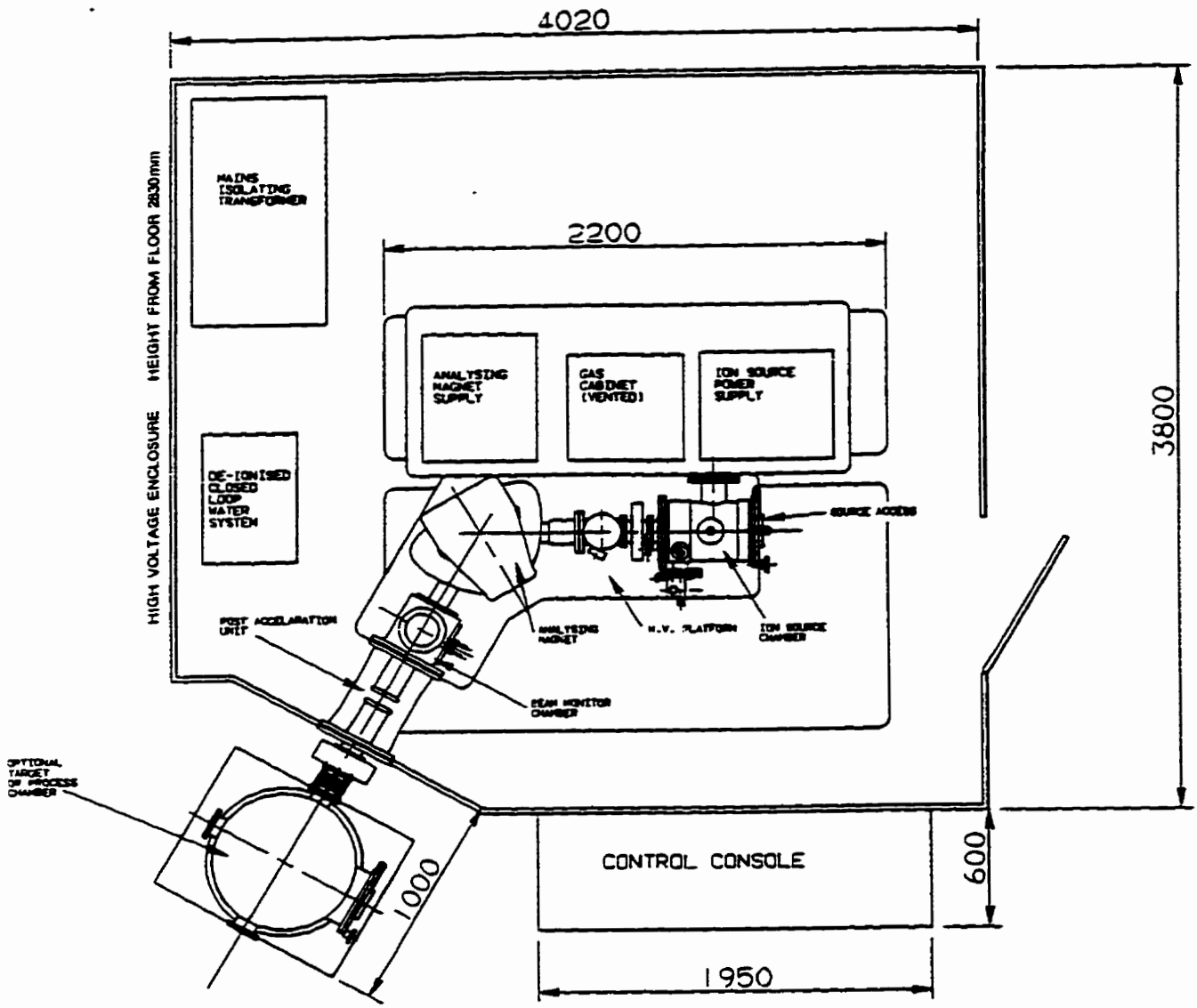

Figure 3.3 Top view schematic of ion accelerator

10^{-6} Torr so ions can be accelerated to very high speed by kilovolts of electrical potentials. Because of the high voltage, these components are placed on a high voltage platform which is isolated from ground by insulator poles as shown in Figure 3.4*. The system is supported by a de-ionized closed-loop water cooling system, gas supply system, vacuum pumps and various power supply systems. Most of these parts, except the target chamber, are placed inside a high voltage enclosure and controlled through a 64 transmitter channel fiber optic control system in order to ensure safety.

The ion source shown in Figure 3.5* is a Freeman ion source with slit extraction. The charged particles are extracted in form of a wedge shaped ion beam. Sharp focused beams of milliampere intensity can be obtained with most materials for stable continuous operation. The ion source is built for operation with two gas lines which is very convenient for my experiment.

The analyzing magnet is a variable geometry magnet which provides 60 degree, 40 cm radius, homogeneous deflecting field in order to analyze different ions. The maximum field strength is over 12,000 gauss. The pole

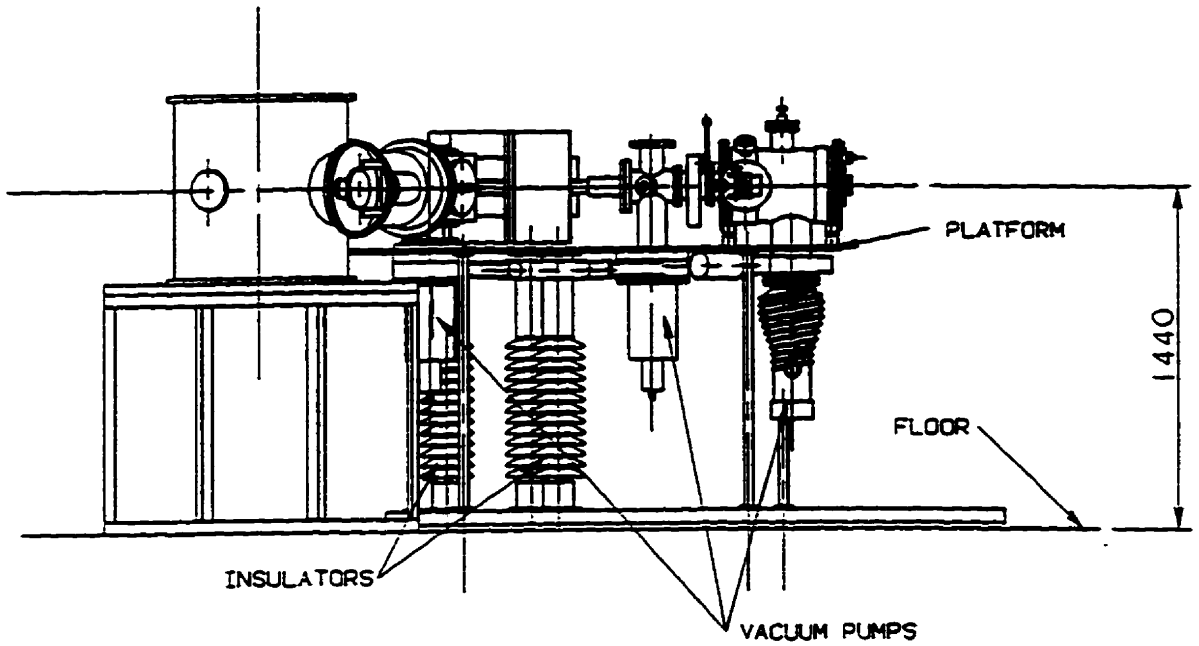

Figure 3.4 Side view schematic of Whickham ion accelerator

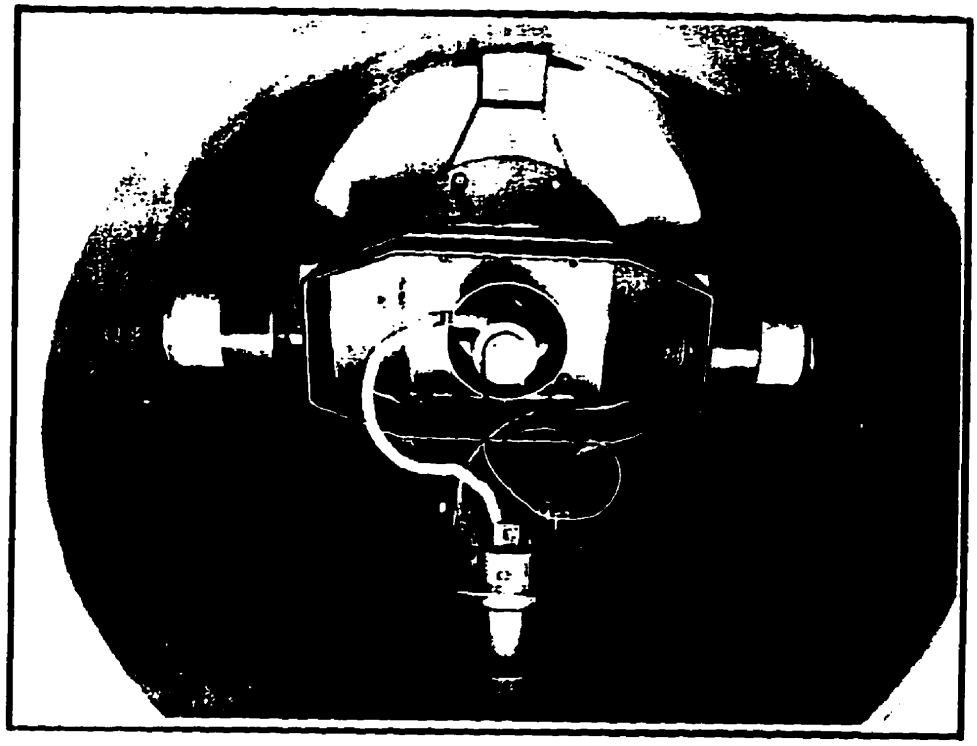

Figure 3.5 The picture of Freeman ion source

gap of the magnet is 5 cm which allows for a 4 cm diameter ion beam to pass through.

Ion bombardment or isotope separation can be carried out in the pre-acceleration work chamber with energy up to 50 keV. However, the working energy is usually fixed to 30 keV in order to maintain system stability. For higher energy ion bombardment, the ions are further accelerated through the post-acceleration column, which employs a single gap lens, to up to 150 keV. This way the total single charged ion energy is up to 200 keV when the ions arrive at the earth potential target chamber.

Four different ions, Deuterium, Helium, Nitrogen and Argon, are used in this experiment. Among them, He^+ and Ar^+ are noble gas ions. The reason of using noble gases is to eliminate a potential chemical reaction between the incident ion and target atom. Energies of ions vary from 10 keV (for helium and deuterium) up to 50 keV (argon and nitrogen) at a step of 10 keV. This is the first time that the Whickham ion accelerator worked at 10 keV since it was installed at McMaster University in 1980. Two fluences, 10^{13} and 10^{14}ions/cm^2 , have been set to for all four ions at energy of 30 keV by properly control the beam current and the bombarding time. One Kapton

sample was bombarded by 30 keV deuterium at fluence of 10^{15} ions/cm^2. The pressure of the target chamber is kept below 10^{-6} Torr by a six inch oil diffusion pump backed with a high capacity mechanical roughing pump through all experiments.

3.3 Surface Analysis by AFM

Many analytical techniques were used to study the surface of polymeric materials. Among them, secondary ion mass spectroscopy (SIMS), Rutherford backscattering spectroscopy (RBS), and X-ray photoelectron spectroscopy (XPS) are the most widely used for studying ion induced radiation damage on polymer. However, all of them have drawbacks of not being able to study spatial change locally and possibly altering the surface by employing energetic ions and X-rays. For surface studies, these technological limitations were not overcome until the invention of the atomic force microscope in 1985.

Atomic force microscopy (AFM) is an important sibling of scanning probe microscopy (SPM). The first SPM was the scanning tunneling microscope (STM) invented by scientists at IBM Zurich Research Laboratory. It was in the late 1970's when Gerd Binnig and Heinrich Rohrer were looking for a technique to study the thin film of oxide layers on metal surface locally. After realizing that by scanning a tip at a proper tunneling current they would be able to obtain topographic data and develop a new microscope, they began investigating how to control the small tunneling current between a sharp tip and conductive surface using piezoelectric

devices. Their success in controlling sample tip spacing at a very small voltage combined with advances in vibration isolation lead to atomic resolution imaging of the surface. In 1983 they successfully produced the first atomic resolution image of two unit cells of the (7 × 7) reconstruction of Si(111)[26]. Binnig and Rohrer received the 1986 Nobel Prize in physics for inventing the STM which can achieve atomic resolution.

Despite of its great success, the application of STM is limited to study the surface of conductive materials. In 1985, when Binnig took a leave from IBM Zurich Laboratory, he went to Stanford University where Binnig, Quate and Gerber invented the atomic force microscope (AFM)[27]. The idea comes from using force, instead of tunneling current, to image the surface. This would overcome a major disadvantage of STM that it can only work on conductive materials. Since it is a common practice to use the displacement of a spring as a measure of force, they estimated the spring constant of the force between atoms and found that by measuring the motion of a tiny cantilever they would achieve atomic resolution without displacing atoms. Shown in Figure 3.6* , the new atomic force microscope design is analogous to a stylus profilemeter but uses a very sharp tip to measure very

* Courtesy of Park Scientific Instruments, Mountain View, CA.

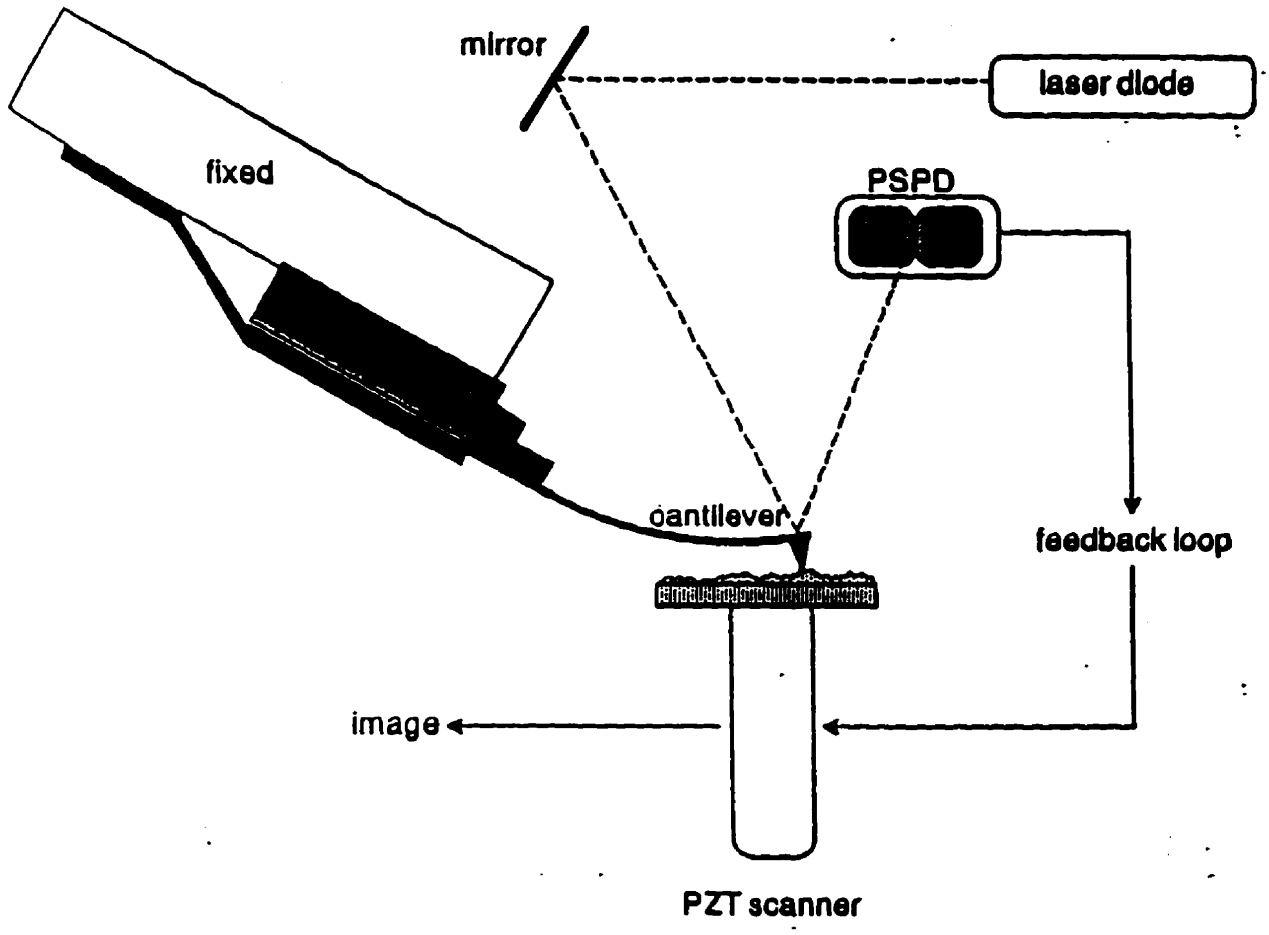

Figure 3.6 Schematic of atomic force microscope

small force between tip and surface. With the technologies obtained from developing STM, they quickly built an AFM that uses a sharp tip mounted on a cantilever of proper spring constant to measure the small force between tip and surface. In the first AFM, a STM has been used to measure the motion of the cantilever.

Because of a similar operating principle, many SPM share components of same function such as piezoelectronic scanner and feedback control system. For a piezoeletronic scanner, most recent models utilize a smart design of a single tube of piezoeletronic materials; four outside electrodes are positioned as quadrants in axial directions, and the 5th one is on the inside wall of the tube. By applying appropriate control voltages to these electrodes, the displacement can be made in all three dimensions at nanometer scale. When the tip approaches the sample, the forces between tip and surface bend the cantilever and the deflection is measured and converted to electronic signals and then sent through a feedback system.

Unlike STM which uses a tunneling current, there are many techniques, i.e. laser interferometry and capacitance measurement, for detecting the cantilever deflection. Most recent AFMs utilize an optical

deflection technique which consists of a segment photodiode (SPD) and a laser beam reflection from the back of the cantilever. In this system, deflection is measured by reflecting a fine laser beam off the back of the cantilever and measures the deflection of the beam by position-sensitive segment photodiode (PSPD).

The feedback control system compares the measured voltage with a user-adjustable "set point" voltage which corresponding to a certain force between tip and surface. If the measured voltage is larger, the feedback control system adjusts the voltage applied on piezotube scanner to lower the sample to maintain constant force, and vice versa. Because the piezoelectronic tubes expand linearly with applied voltage, the control voltage to maintain a constant force is directly proportional to the vertical changes in tip position. This signal, which represents the change of surface height at that point, is stored in computer. For each single scan, a cross-section profile is produced. A two dimensional image of surface topography is obtained after scanning over a small surface area.

As shown in Figure 3.7, the AFM used in this experiment is a SFM-BD2 scanning force microscope designed and built by Park Scientific Instruments of Mountain View, California. It is an ambient AFM designed

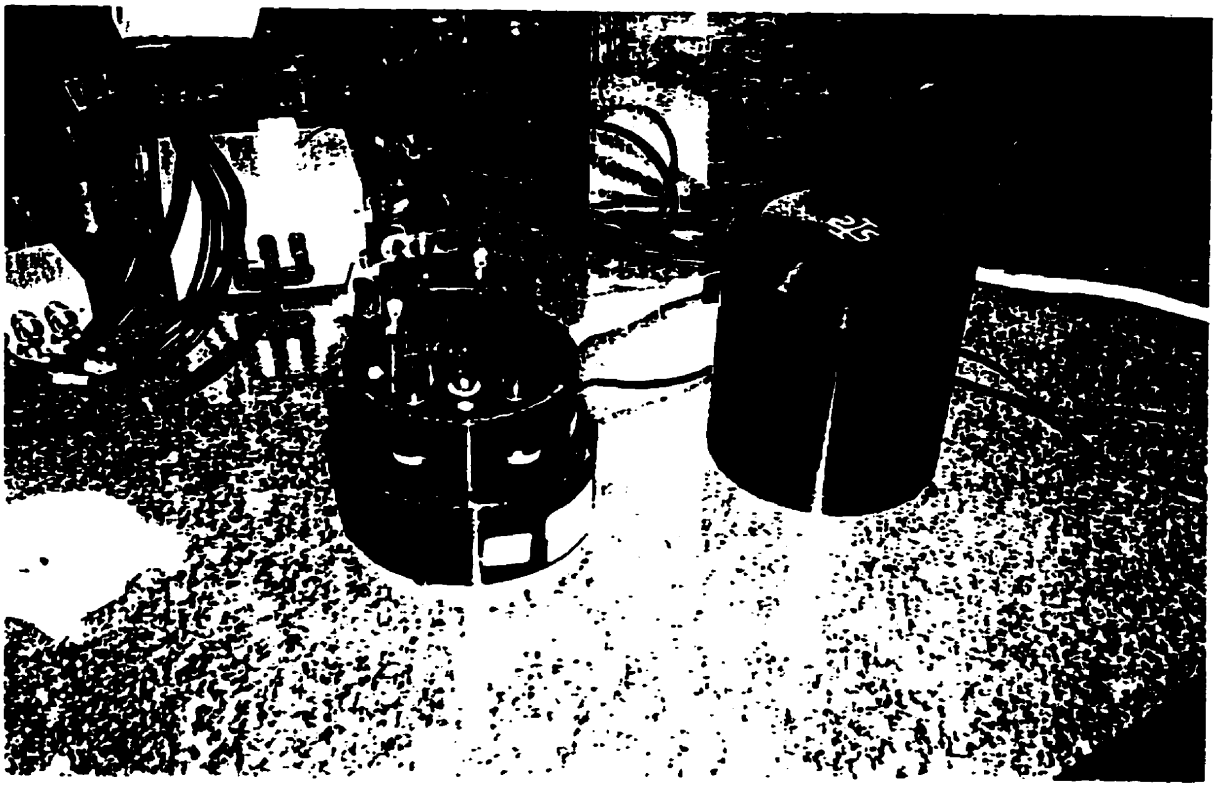

Figure 3.7 A picture of SFM-BD2 microscope

to work in contact mode. In most cases, vibration control is achieved by its own rigid and compact structure. The system is shown in Figure 3.8*. Instead of using a HP workstation, control electronics and the software from Park Scientific Instruments, a Powerland 486 DX 66MHz PC, customer-built electronic controller and control software are used. The atomic force microscope consists of two main parts: the microscope base and microscope head. The piezotube scanner and a pico drive stepper motor are in the microscope base for controlling the positions. The microscope head shown in Figure 3.10* houses laser, position-sensitive photodetector (PSPD) and the cantilever mount. A chip cut from a silicon wafer with V-shape cantilevers, each of them has a standard pyramid shaped silicon nitride tip as shown in Figure 3.11, is held in place on the cantilever mount by a small clip. The whole system has been calibrated by measuring a 1μm × 1μm grating.

The Kapton sample is cut to 0.5 × 0.5 cm^2 size and attached on the sample holder by double-sided tape. The sample holder is fastened into the sample mount by a set screw which can be adjusted by a jeweler's handle Allen key. Other fine adjustments of laser beam and tip-sample position are

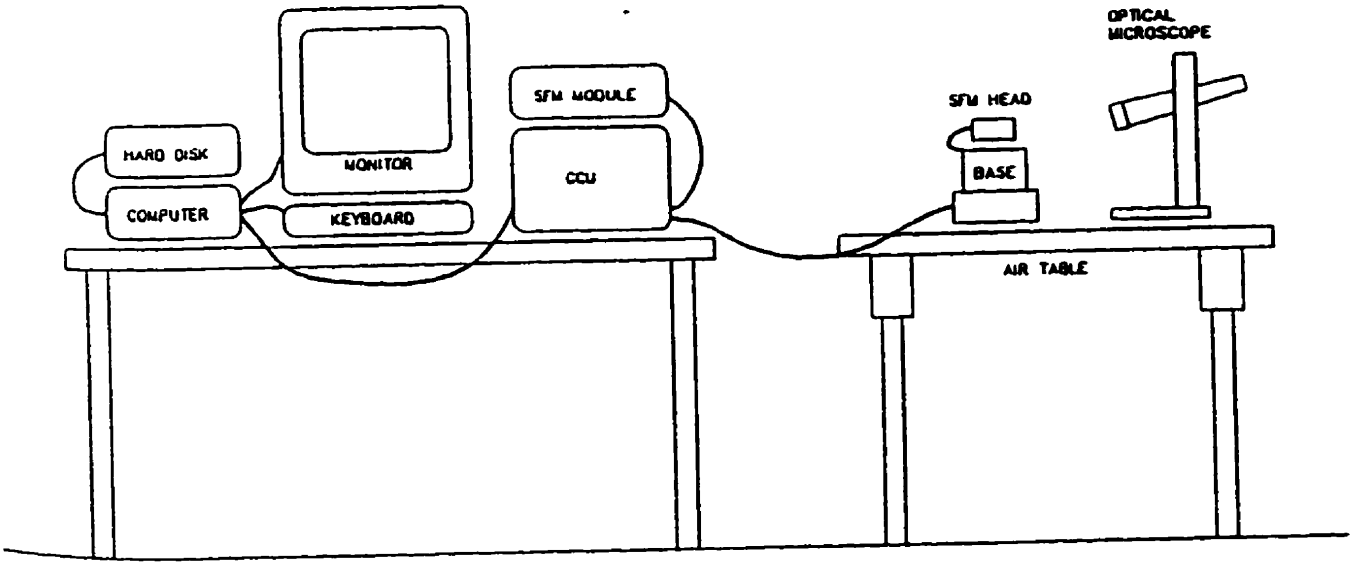

Figure 3.8 Schematic of AFM and control system (Courtesy of Park Scientific Instruments Ltd.)

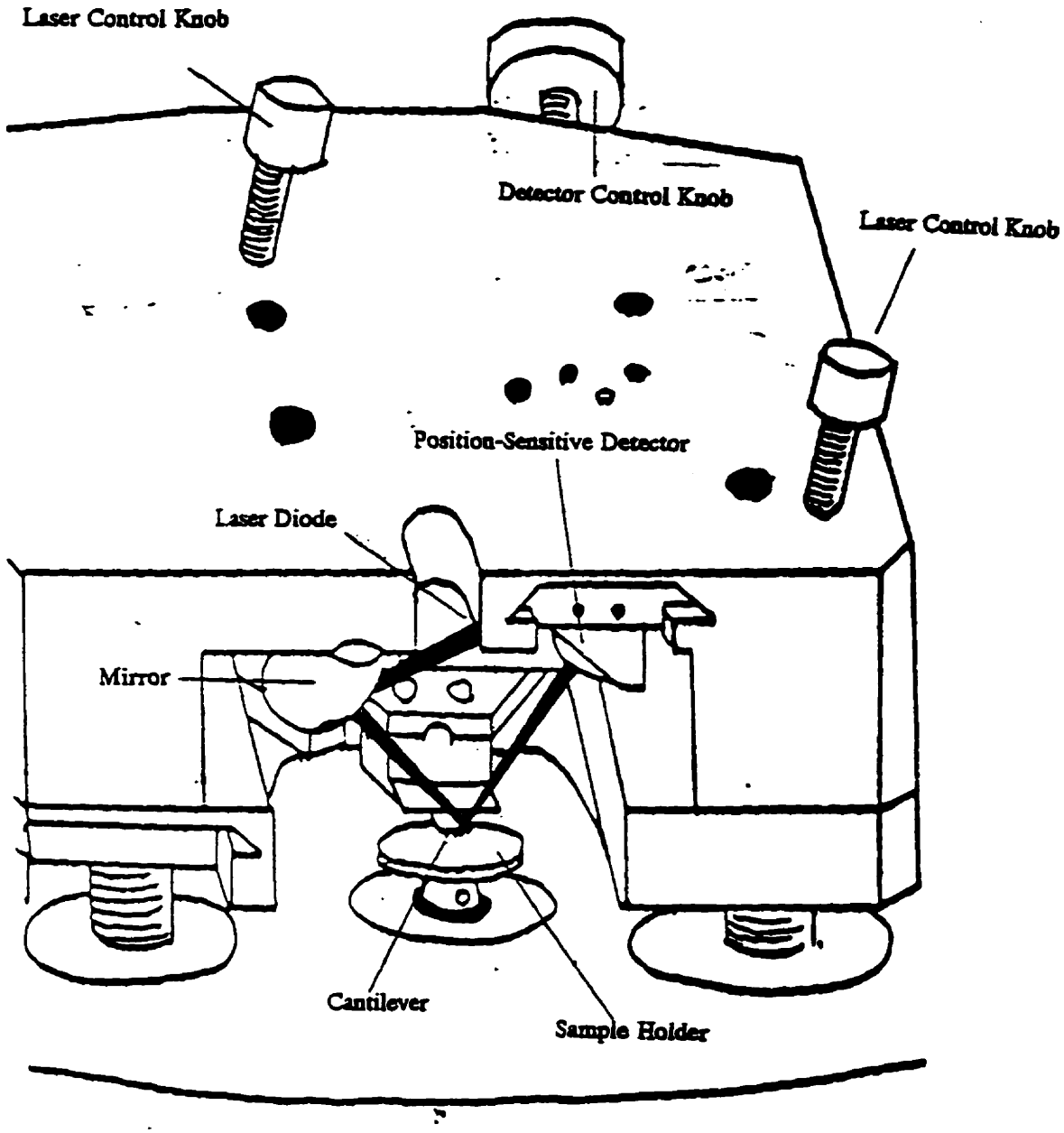

Figure 3.10 The head of SFM-BD2 microscope. The sensibility of the deflection sensor is 1.6 mV/nm (Courtesy of Park Scientific Instruments).

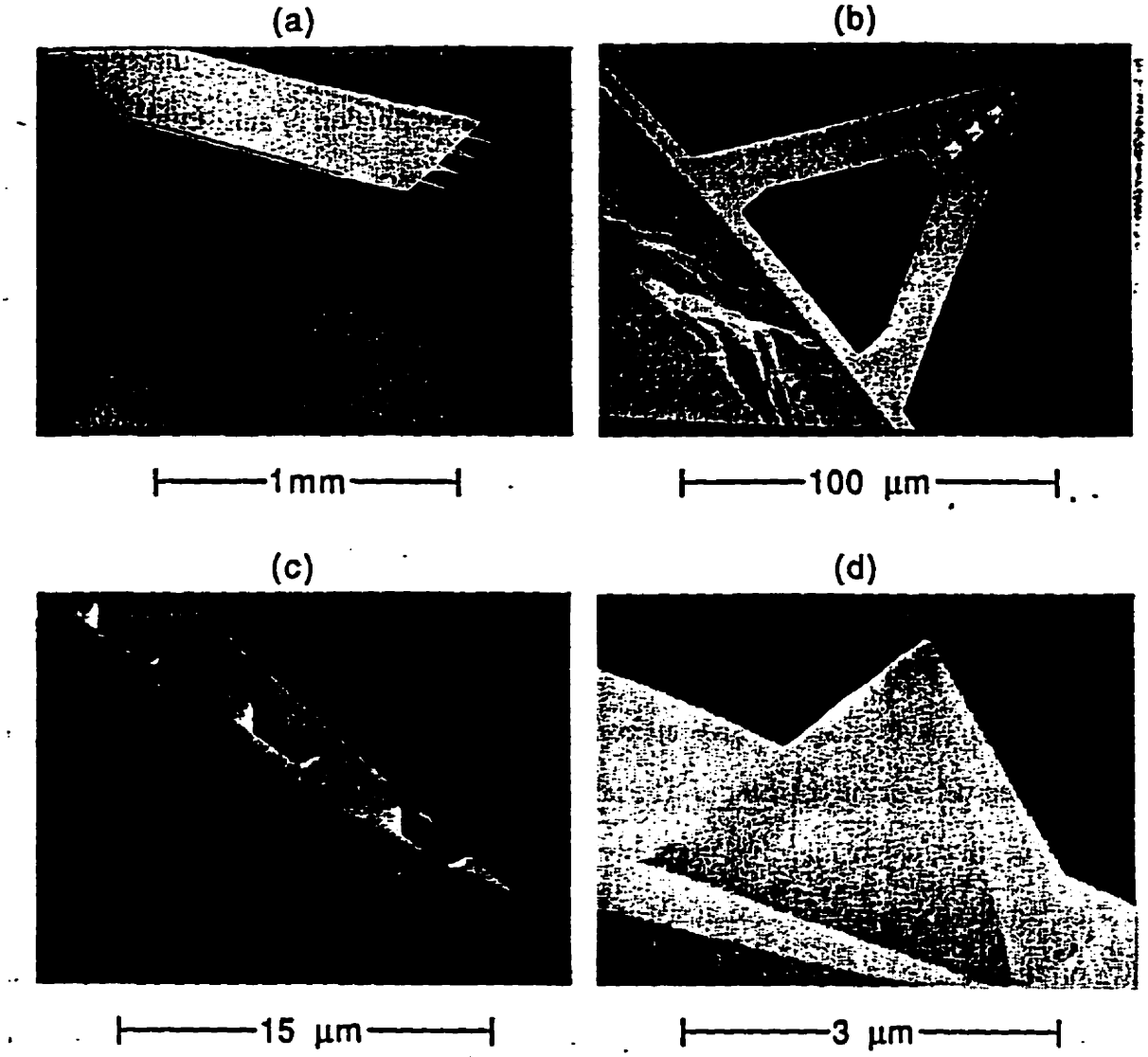

Figure 3.11 The standard silicon nitride tip for AFM. The tip is of pyramid shape with a radius of curvature of 30 nm at the very end .

performed under a binocular optical microscope with lightening from a fiber optic lamp. Fine tip approach is achieved by stepper motor which is controlled by computer. The maximum scan size is 11 μm × 11 μm for this SFM-BD2 atomic force microscope. A scanning scheme is developed to scan the surface systematically.

Chapter 4 Results and Discussion

4.1 Surface Topography

After being bombarded by energetic ions, the surface topographic changes on polymer have been investigated. There are many different types of features resulted on the surface which depends on the incident ions (energy, fluence, mass and charge state) and polymer specimen (composition and structure). Despite of lines, the most common features are the craters and hillocks found on ion bombarded polymer surface. Because of the complex structure and composition of polymeric materials, the mechanisms of forming these features are still unclear. Many different models are proposed while trying to solve this question.

Previous research indicates that, unlike ion damage on metals, radiation causes scission and crosslink of polymer chains which usually alter the structure and composition of the polymer[28a, b]. Strong evidence of a polymer undergo chain scission and crosslink was the change of molecule weight after ion bombardment. Besides directly measuring the molecule weight, the change of solubility is a good indicator of molecule

weight change. The most interesting chemical change related to radiation damage on polymer is the release of free radicals and gases after ion radiation. This study suggests that diffusion and trapping of free radicals and gases in ion bombardment damaged polymer may play the most important roles on observed crater formation.

First of all, the pristine Kapton film is analyzed by AFM. Lines of different orientations are observed on other wise smooth surface as shown in Figure 4.1. There is no other type of feature found on the surface of pristine Kapton films. These lines can be simply interpreted as scratch lines[29]. It is noticed that the optical reflection of the film is slightly different from one side to another. After both sides are examined by AFM, more lines have been observed from the rough side. This interesting phenomenon also indicates that these lines are scratch lines.

It has been reported that scanning of the tip at a rather large force may result in surface modification of the polymer[30]. This effect has happened only once when I was taking an image on Kapton. Another interesting phenomena is sometimes a wave pattern, which resembles wave patterns found on a sand beach after the tide retreats, appears on image as shown in Figure 4.5. It is originally considered to be another modification effect on

Figure 4.1 Scratch lines observed from Kapton surface by AFM. The size of image area is 4×4 μm^2.

Figure 4.2 Ion induced damage on Kapton surface. The size of image area is 2300×2300 nm^2.

polymer caused by the tip. However, this pattern disappears when the system is shut down and restarted again to scan the same area. Therefore, it may be caused by electronic noises.

The craters have been observed from ion bombarded polymers as well as highly oriented pyrolytic graphite (HOPG) surface[32a, b]. However, the mechanism of crater formation is still not clear. In this study, craters of various diameters and depths have been found on ion bombarded Kapton surface. It is noteworthy that most of these craters are circular in shape and having rims as shown in Figure 4.2, Figure 4.3 and Figure 4.4. These unique features may provide a key for understanding the formation of craters. The mechanism of crater formation is discussed in detail at the end of this chapter.

As scratch lines, hillocks on ion bombarded polymer surface have been reported by previous studies[33]. In this research, hillocks of different size are frequently observed on the surface but these areas are usually avoided in order to have a better look at craters. Barlo Daya et.al. report that conical-shaped hillocks having nearly circular shaped bases are observed

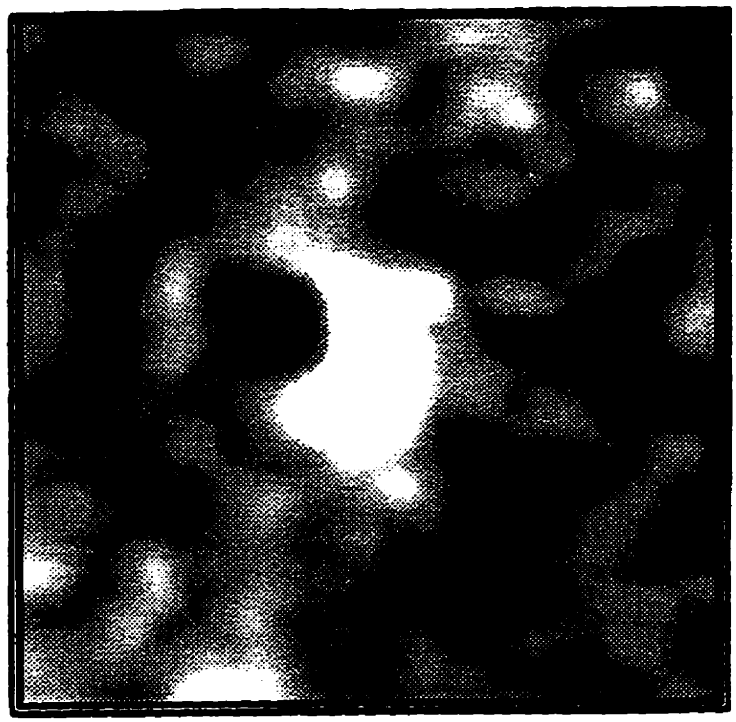

Figure 4.3 Crater formed on 20 keV Ar^+ ion bombarded Kapton surface The size of image area is 280×280 nm^2.

Figure 4.4 Crater formed on 20 keV He^+ ion bombarded Kapton surface. The size of image area is 280×280 nm^2.

from 78.2 MeV ^{127}I bombarded mica surface[34]. Since these hillocks can be erased by probe tip and reveal craters, they suggest that the hillocks could be thick blisters created by hydrodynamic pressure. The mechanism of crater formation is discussed in detail at the end of this chapter.

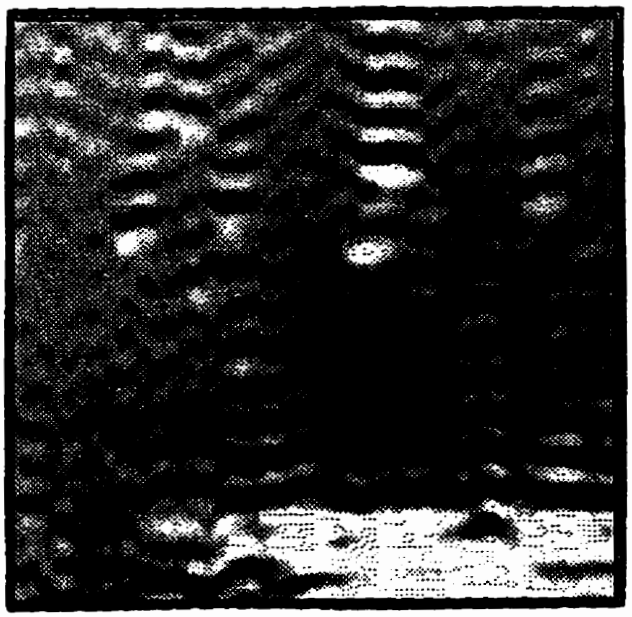

Figure 4.5 The wave pattern observed on Kapton surface. The size of image area is 1.7×1.7 μm^2.

4.1 Depth and Range

The major advantage of the ion beam technique lies on the high controllability of all parameters associated with incident ions. By precisely controlling the incident ion energy, scientists and engineers are able to control the ion bombardment induced results in solids. This has attracted a great amount of interests from both semiconductors and spacecraft industries.

The depth and range are the most important factors in studying stopping ions in matter. Compared to the crater formation on an ion bombarded surface, the theory of ion penetration depth and ion range is well developed. The calculations of penetration depth and range in polymers are based on ZBL theory of stopping power and range explained in Chapter two. By using the TRIM program, depth and range of different ions in varies polymer materials can be easily calculated. Although the discrepancy between calculated and measured range in polymer is larger than in metals, it is still considered to agree well in terms of basic trend. The success of ZBL theory on polymers gives us a very important guide for understanding the mechanism of ion induced damages on polymers.

In this work, the depth and range of ions in a polymer as a function of energy is investigated by bombarding the Kapton films with different energy ions. The effects of ion mass and fluence have also been studied. Because of the low energy, most of the ion induced damage results on the surface or near surface region. The depth of ion damage is directly measured by atomic force microscopy (AFM). Figure 4.6 and Figure 4.7 show both measured and calculated depths as a function of ion energy for N^+ and Ar^+ ions. It is noteworthy that all the measured depths are smaller than calculated by TRIM. This effect is more significant for N^+ ions than Ar^+ ions. Shown in Figure 4.8 is the damage depth, which is caused by 30 keV ions, as a function of ion mass. In this study, the discrepancies between measured and calculated depths vary from around 30% for nitrogen and argon to over 50% for deuterium and helium. Similar effects have been discussed in previous works [35, 57].

Since the depth calculated by TRIM is the depth at which the incident ions are initially stopped in a polymer, the results indicate that there is a strong trend of diffusion towards the surface. The diffusion of hydrogen and helium in ion bombarded polymers has been studied [36a, b]. It concludes

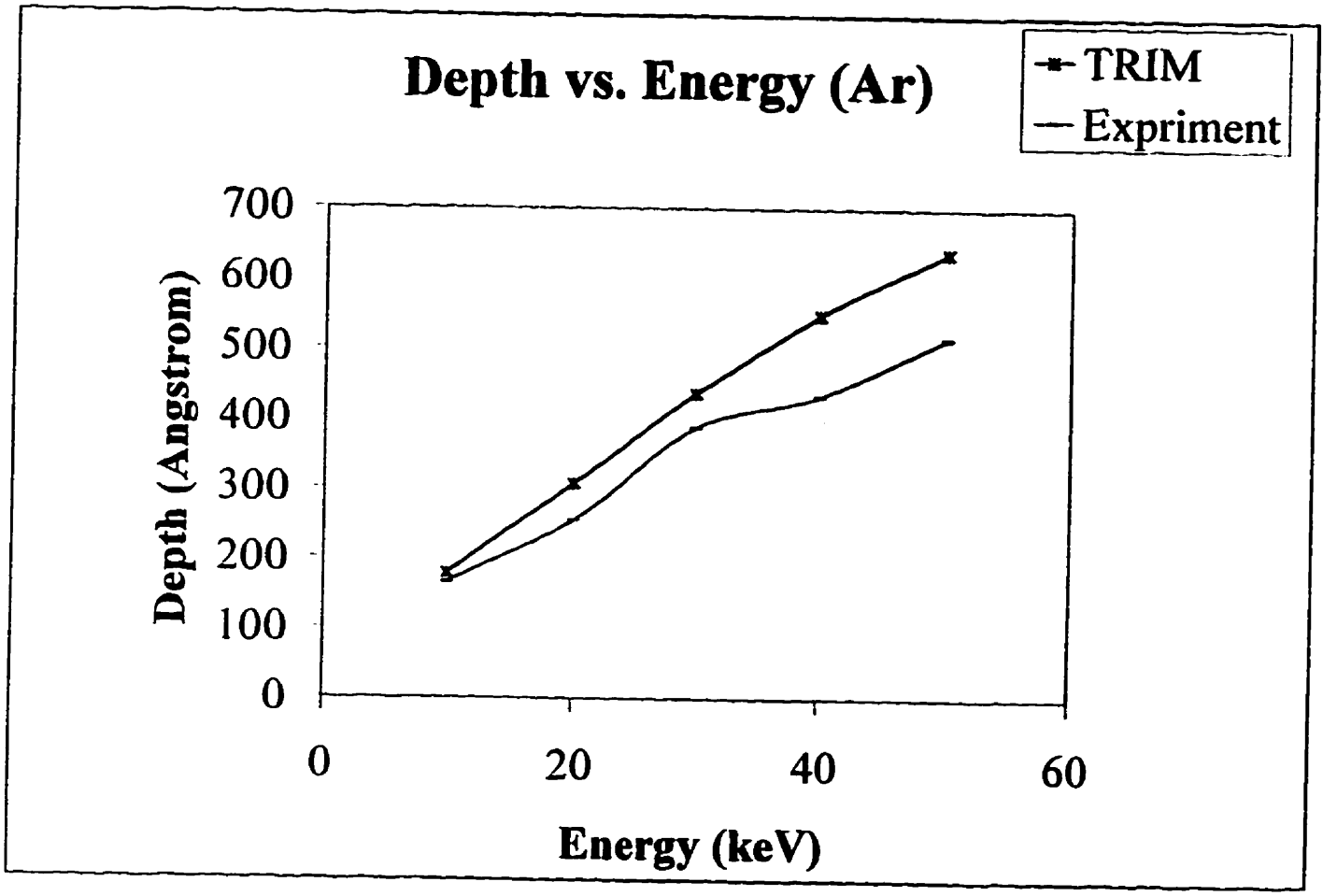

Figure 4.6 Depth vs. energy for Ar^+

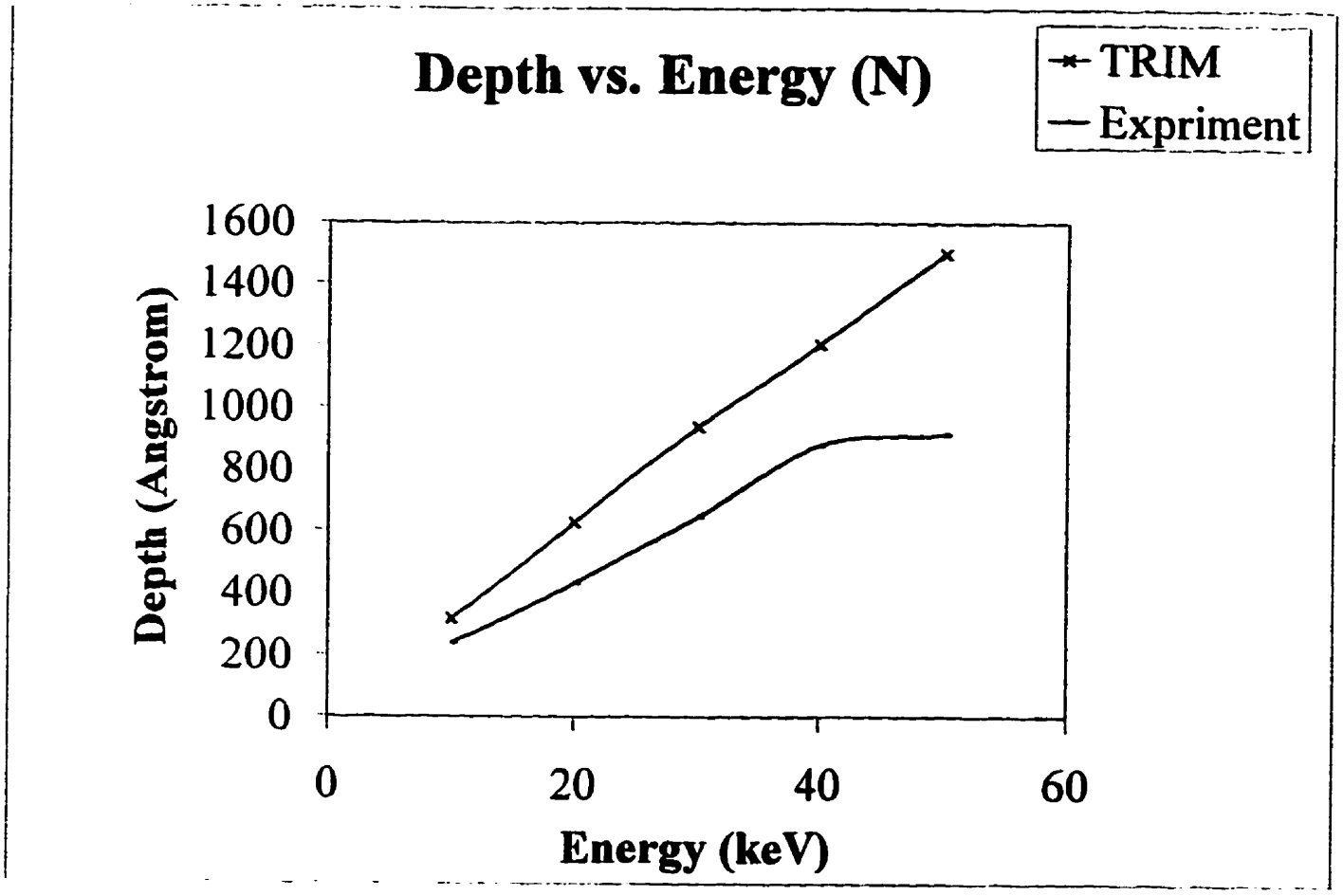

Figure 4.7 Depth as a function of energy for N^+

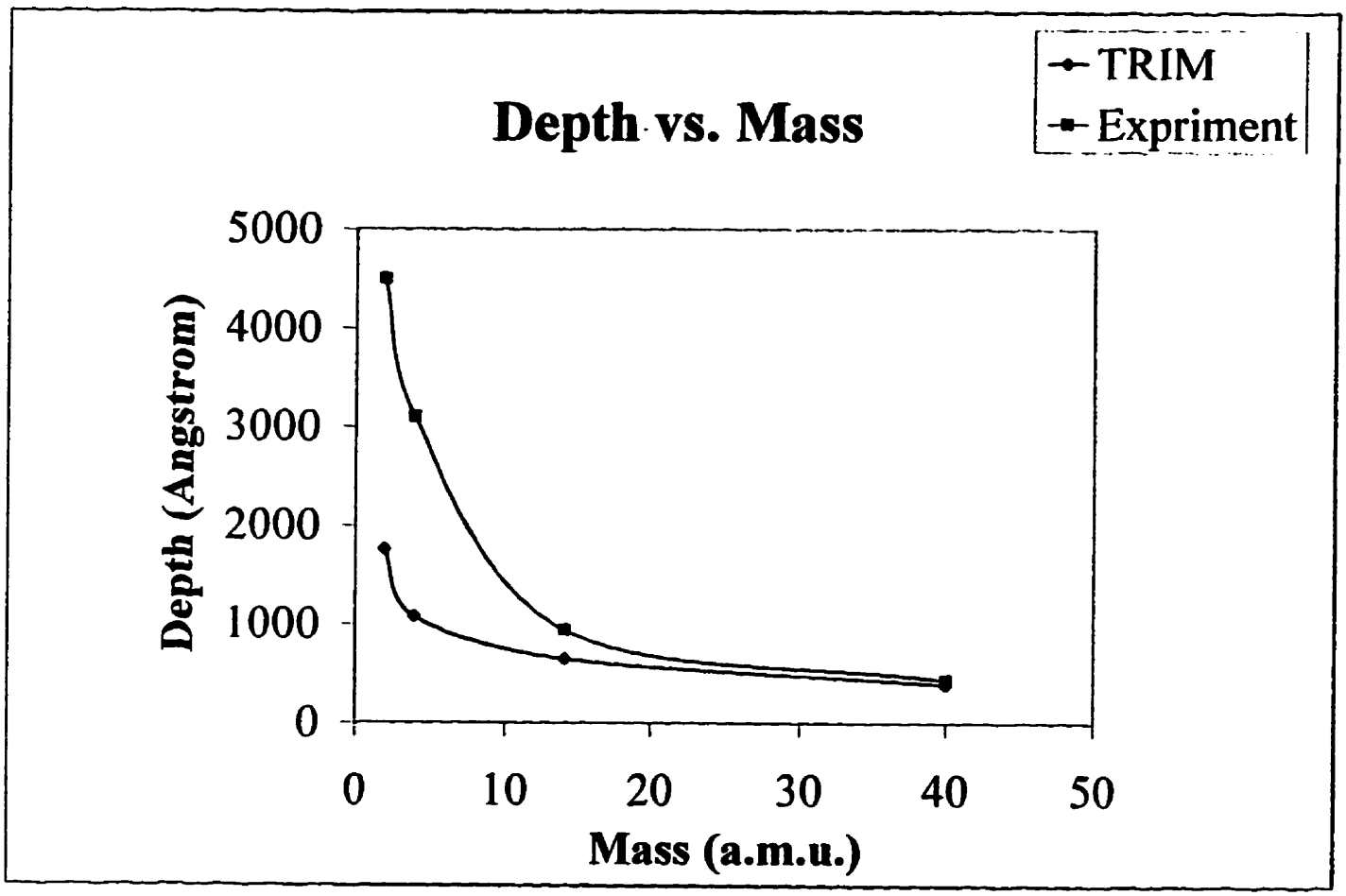

Figure 4.8 Depth as a function of ion mass for 30 keV ions

that the diffusion coefficient of helium is not less than $10^{-14}cm^2/s$[61]. The results of this study strongly support the existence of diffusion effects in polymer as suggested by the previous study. Since the discrepancies are quite large in both cases, it seems that diffusion and thermal effects need to be evaluated in addition to the TRIM calculation of final ion distribution in low energy ion bombarded polymer. The effects of surface, diffusion and trapping, which play important roles in ion induced damage to polymer, need to be further investigated and included in range calculation. However, the mechanism is so complicated that it is not yet completely understood.

4.1 Crater Formation

Crater formation on ion bombarded surfaces has been studied since the late 1960's. Most of the early experiments are on high energy He^+ and D^+ ion bombarded metals at high fluence. The energy varies from 160 keV to 80 MeV and the fluence from 10^{17} t0 10^{18} ions/cm^2. Usually high temperature is also a prerequisite. The measurement of gas release rate indicates that initially a large fraction of the incident ions is trapped by the surface[37]. Since only a small fraction of blisters breaks at above fluences, the number of craters formed on metal surfaces is very small in most cases. Similar effects seem to occur on ion bombarded polymer surfaces at room temperature. The study of surface topographic change on ion bombarded polymers started in the late 1980's after AFM was introduced as a powerful technique for surface analysis. The crater formation on polymer surface has been widely reported [38]. The mechanism of crater formation on polymer is still unclear. There are different models to explain the formation of craters on polymer surfaces. Among them, the pressure pulse model, and the thermal spike model are widely cited[39, 40, 41].

The pressure pulse model is a hydrodynamic type model. In the pressure pulse model, the angular distributions of target molecules are non-symmetrical and the energy density resulting from the ion-solid interaction propagates in solid by diffusion. The thermal spike model assumes that the energy deposited by incident ion creates a thermal spike characterized by a temperature, and the energy is transported in solid due to heat conduction. The third model, shock wave model, suggests that the target molecule redistribution is due to a propagating shock wave which is caused by the sudden pressure change in the ion bombarded region[42]. All three models consider energy transfer in the solid but only the first model treats the energy transfer as a result of mass transport in the solid. However, mass transport is very important in understanding the crater formation mechanism.

In this research, craters have been observed from an ion bombarded polyimide Kapton surface as shown in section 4.1. The size of the crater is so large compared to the size of incident ion that they could not be formed by a single ion impact. The cross-sections of these craters are studied by AFM. In addition to the characteristic circular shape and rim, most of these craters have unique depth profiles as shown in Figures 4.9. and 4.10. As

discussed in the previous section, the crater depth changes accordingly with incident ion energy but is always shallower than calculated by TRIM. Considering gas release and diffusion effects in the ion bombarded polymer, it appears diffusing ions and released gases play an important role in crater formation.

When polyimide is bombarded with ions, there are released gases (H_2, CH_4, CO, CO_2) in the target as a result of chain scission[51,55]. The incident ions also create a great number of defects[56]. For instance, one 30 keV N^+ ion can create 197 defects in a Kapton target according to TRIM calculation. These gases are moving inside the target through diffusion and can be trapped by defects to create cavities[52]. This diffusion-trapping process may form the foundation of the crater formation mechanism[47,53]. Therefore, a model is proposed based on this process as shown in Figure 4.11.

The process includes diffusion and trapping of gases, forming bubbles on the surface, breaking of blisters with gas release, and eventually forming craters on the surface. Initially, incident ions create defects and cause chain scissions which release free radicals and gases. The incident ions may also capture electrons to become gas atoms or molecules. These

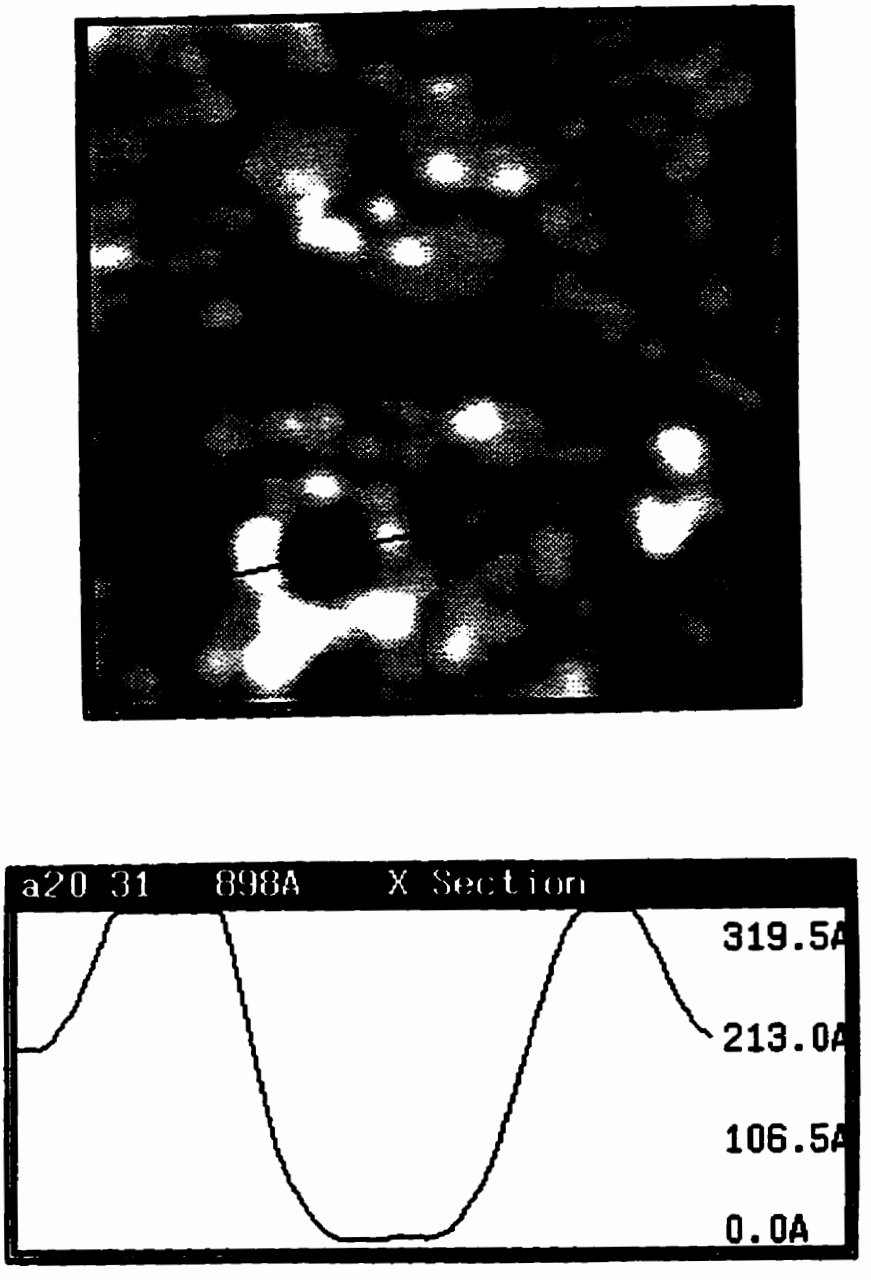

Figure 4.9 The cross-section of crater caused by 20 keV Ar^+ ions. The image area is 280×280 nm^2.

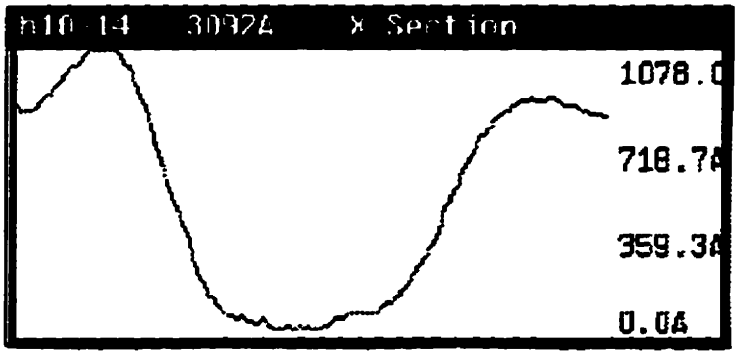

Figure 4.10 The cross-section of crater caused by 10 keV He^+ ions. The image area is 570×570 nm^2.

gases diffuse in polymers and are trapped by defects to form bubbles. While the concentrations of gas build up, the coalescence of bubbles forms blisters. The internal pressure on the surface causes surface deformation and eventually breaks the blister. This crater, with a depth close to the projected range of incident ions, is formed and gas is released. After gas release, the ruptured surface collapses to form the unique cross-section as shown in Figures 4.9 and 4.10. Although more research needs to be done in order to further evaluate this model, so far it has explained most phenomena, such as the shallower depth and damage profile observed on ion bombarded Kapton.

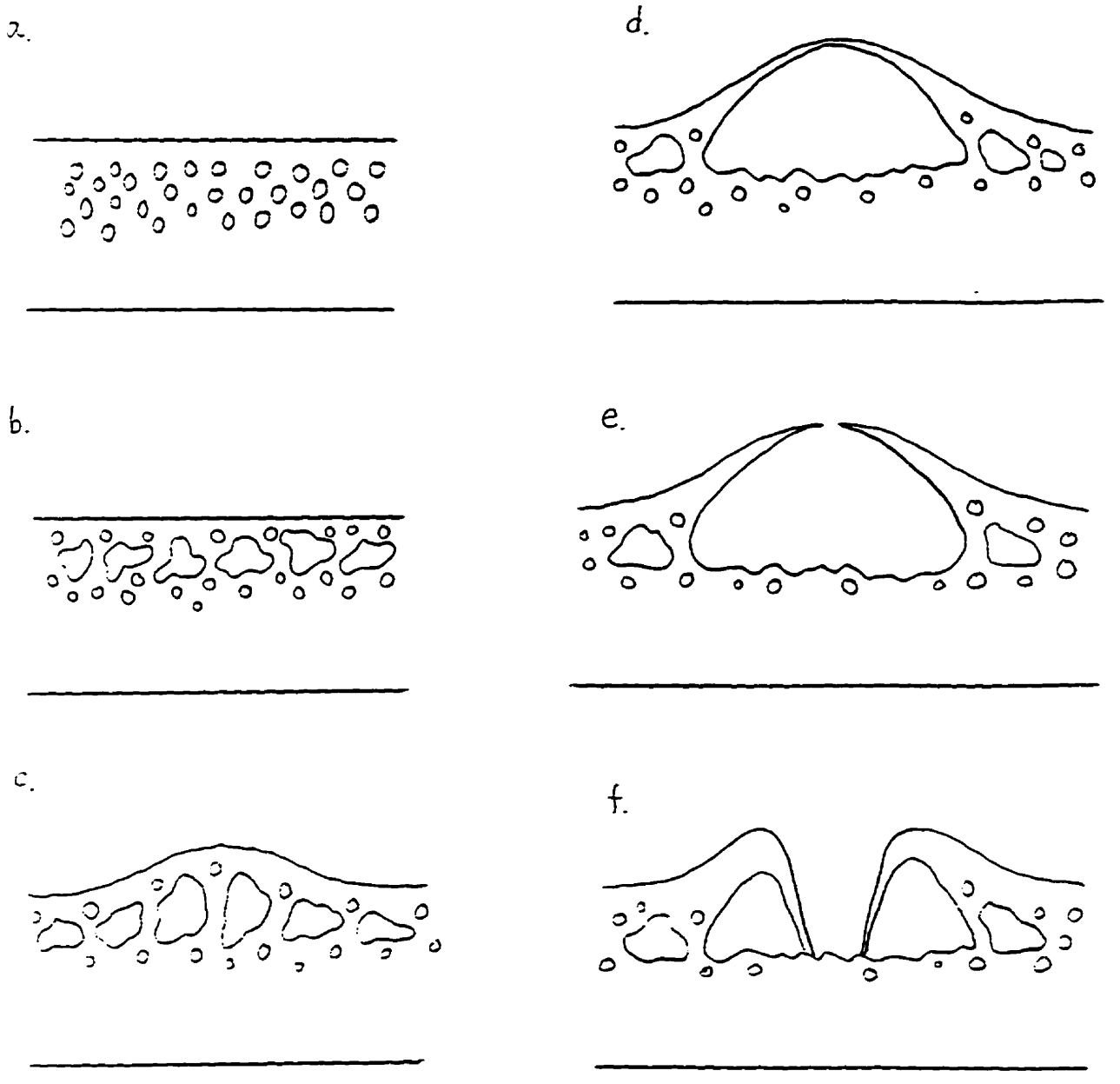

Figure 4.11 Schematic of crater formation on polymer surface. a. defects created by ions; b. gas trapped by defects; c. surface deformation caused by bubbles; d. blister formed by the coalescence of bubbles; e. rapture of blister and release of gas; f. surface collapses to form crater

Chapter 5 Summary and Conclusions

In this research, ion induced radiation damage on polyimide Kapton surface has been studied by atomic force microscopy (AFM). Different types of surface topographic changes have been observed. The depths of surface damages are directly measured and then compared with TRIM calculations. The mechanism of crater formation is investigated and a model based on diffusion is proposed. The conclusions are as follows:

(1). Craters are formed on the Kapton surface by low energy ion radiation at a fluence from 10^{13} ion/cm^2 to 10^{15} ions/cm^2.

(2). The depth of ion damage changes as a function of incident ion energy and ion mass while the fluence seems has no impact on damage depth.

(3). The calculated ion depths by TRIM program appear to be larger than measured probably because the diffusion effect is not included in the ZBL theory on which the TRIM program is based.

(4). The unique cross-section of the crater and depths shallower than the calculated suggest that the crater formation results from burst blister according to the proposed model.

(5) Both incident gaseous ions and released gas from chain scission must play a role in crater formation through diffusion in the ion bombarded polymer and trapping by defects.

Further research to study the ion radiation effects on polymers may include: (1) different chemical structures and compositions, (2) ion induced chemical change by real-time analysis techniques, (3) the effects of temperature, fluence and flux, (4) the radiation damages caused by heavier ions and non-gaseous ions.

Bibliography

(1a) R. Wang, J. L. Brimhall, Materials Research Society Symposia Proceedings, Vol.27, p729-734

(1b) L. E. Pope, F. G. Yost, D. M. Follstaedt, S. T. Picraux, J. A. Knapp, Materials Research Society Symposia Proceedings, Vol.27, p.661-666

(2) C. R. Kalil, P. R. Yong, Instrumentation in the Aerospace Industry: Proceeding of the international symposium, 1993, Instrument Society of America, p. 445-449

(3) T. Feder, Physics Today, Feb., 1997, p.60-61

(4) S. Miyake, S. Watanabe, H. Miyazawa, M. Murakawa, R. Kaneko, T. Miyamoto, Appl. Phys. Lett., 65 (25), 1994, pp. 3206-3208

(5) B. Soder, J. Roth, W. Moller, Nucl. Instr. and Meth., B32 (1988) 160-165

(6) J. R. Fried, Polymer Science and Technology, Prentice-Hall Inc., 1995

(7) G. Binnig, H. Rohrer, Rev. Mod. Phys., 59, 1987, p.615

(8a) D. Fink, M. Muller, L. T. Chadderton, P. H. Cannington, R. G. Elliman and D. C. McDonald, Nucl. Instr. and Meth. B32 (1988) 125

(8b)J. Davenas, G. Boiteux, X. L. Xu, and E. Adem, Nucl. Instr. and Meth. B32 (1988) 136-141

(9) M. S. Mathur, J. S. C. McKee, M. Liu, D. He, Materials Science and Engineering B, 1997

(10) N. Bohr, Phil. Mag. 25, 10, 1913

(11a) H. A. Bethe, Z. F. Physik, 76, 293, 1932

(11b). F. Bloch, Z. F. Physik, 81, 363, 1933

(12a) N. Bohr, Phys. Rev., 58, 654, 1940

(12b) N. Bohr, Phys. Rev., 59, 270, 1941

(13) J. Lindhard, Mat. Fys. Medd. Dan. Vid. Selsk., 28, No.8, 1954

(14a) David K. Brice, Ion Implantation Range and Energy Deposition Distribution, Vol.1, IFI/Plenum, New York, 1975

(14b) K. B. Winterton, Ion Implantation Range and Energy Deposition Distribution, Vol.2, IFI/Plenum, New York, 1975

(15a) J. F. Ziegler, Handbook of Stopping Cross-sections for Energetic Ions in All Elements, Pergamon Press, New York, 1980

(16) J. P. Biersack, L. G. Haggmack, Nucl. Instr. and Meth., Vol.174, 257, 1980

(17) J. F. Ziegler, Ion Implantation Science and Technology, Academic Press, Inc., New York, 1984

(18) J. F. Ziegler, The Stopping and Range of Ions in Solids, Pergamon Press, New York, 1984

(19a) R. B. Guimaraes, M. Behar, R. P. Livi, I. P. De Souza, F. C. Zawislak, D. Fink, and J. P. Biersack, Nucl. Instr. and Meth. B19/20 (1987) 882-886

(19b)M. R. Herberts, P. F. P. Fitchner, M. Behar, Nucl. Instr. And Meth. B111 (1996) 12-16

(20) J. J. Thompson, Phil. Mag., 6-23, 449, 1912

(21) J. F. Ziegler, J. P. Biersack, U. Littmark, The Stopping and Range of Ions in Solids, Pergamon Press, New York, 1984

(22) J. Lindhard, Mat. Fys. Medd. Dan. Vid. Selsk., 28, No.8, 1954

(23) W. Brandt, M. Kitagawa, Phys. Rev., 25B, 5631, 1982

(24) J. F. Ziegler, TRIM Version 95.4, March 8, 1995

(25) R. T. Reeve, J. Of Spacecraft and Rockets, V28, n2, Mar-April, 1992, p.130

(26) G. Binnig, H. Rohrer, C. Gerber, W. Weibel, Phys. Rev. Lett., 1983, 49, 57

(27) G. Binnig, C. F. Quate, C. Gerber, Phys. Rev. Lett., Vol.54, 1986, p.930

(28a) A. Licciardello, O. Puglisi, L. Calcagno and G. Foti, Nucl. Instr. And Meth. B32 (1988) 131-135

(28b) R. Endrst, V. Svorcik, V. Rybka, and V. Hnatowicz, Radiation Effects and Defects in Solids, 1995, Vol. 137, pp. 25-28

(29) Y. Zhu, L. Wang, Z. Lu, Y. Wei, X. X. Chen, J. H. Tang, Appl. Phys. Lett. 65 (1) 1994, pp. 49-51

(30) Q. Zhong, D. Inniss, K. Kjoller and V. B. Elings, Surface Science Letters, 290 (1993), L688-L692

(31) S. Miyake, S. Watanabe, H. Miyazawa, M. Murakawa, R. Kaneko, T. Miyamoto, Appl. Phys. Lett., 65 (25), 1994, pp. 3206-3208

(32a) G. Brauchle, S. Richard-Schneider, D. Illig, R. D. Beck, H. Schreiber, M. M. Kappes, Nucl. Instr. And Meth. B112 (1996) 105-108

(32b) T. Seki, T. Kaneko, D. Takeuchi, T. Aoki, J. Matsuo, Z Insepov, I. Yamada, Nucl. Instr. And Meth.,B121 (1997) 498-502

(33) J. Eriksson, J. Kopniczky, G. Brinkmalm, R. M. Papaleo, P. Demirev, C. T. Reimann, P. Kakansson, B. U. R. Sundqvist, Nucl. Instr. And Meth. B101 (1995) 142-147

(34) D. D. N. Barlo Daya, A. Hallen, P. Hakansson, B. U. R. Sundqvist, C. T. Reimann, Nucl. Instr. And Meth. B103 (1995) 454-465

(35) R. B. Guimaraes, M. Behar, R. P. Livi, I. P. De Souza, F. C. Zawislak, D. Fink, and J. P. Biersack, Nucl. Instr. and Meth. B19/20 (1987) 882-886

(36a) M. B. Lewis, W. A. Coghlan, J. Nucl. Mater. 228 (1996) 302-317

(36b) R. F. Haglund Jr., M. H. Mendenhall, N. H. Tolk, G. Betz and W. Husinsky, Nucl. Instr. And Meth., B32 (1988) 321-330

(37) R. Behrisch, et.al., Ion Surface Interaction, Sputtering and Related Phenomena, Gordon and Breach Science Publishers, London, 1972

(38) T. Seki, T. Kaneko, D. Takeuchi, T. Aoki, J. Matsuo, Z Insepov, I. Yamada, Nucl. Instr. And Meth.,B121 (1997) 498-502

(39) J. Eriksson, J. Kopniczky, G. Brinkmailm, R. M. Papaleo, P. Demirev, C. T. Reimann, P. Hakansson, B. U. R. Sundqvist, Nucl. Instr. and Meth., B101, 1995, p142-147

(40a) R. E. Johnson, B. U. R. Sundqvist, A. Hedin, D Fenyo, Phys. Rev., B40, 1989, 49

(40b) D. Fenyo, R. E. Johnson, Phys. Rev., 1992, p.5090

(41a) I. S. Bitensky, E. S. Parilis, Nucl. Instr. and Meth., B21, 1987, 26

(41b). J. F. Mahoney, J. Perel, T. D. Lee, P. A. Martino, P. Williams, J. Am. Soc. Mass Spectrom, 3, 1992, 311

(42a) A. Mozumder, Adv. Radiat. Chem., 1, 1969, 1

(42b) R. R. Lucchese, J. Chem. Phys., 86, 1987, 443

(43) L. P. Biro, J. Gyulai, K. Havancsak, Nucl. Instr. And Meth. B112 (1996) 270-274

(44) S. L. Koul, I. D. Campbell D. C. McDonald, T. Chadderton, D. Fink, J. P. Biersack and M. Muller, Nucl. Instr. And Meth. B32 (1988) 186-193

(45) C. Trautmann, W. Bruchle, R. Spohr, J. Vetter, N. Angert, Nucl. Instr. And Meth. B 111 (1996) 70-74

(46) Y. Suzuki, M. Kusakabe, M. Iwaki, M. Suzuki, Nucl. Instr. And Meth. B32 (1988) 120-124

(47) V. Hnatowicz, J. Kvitek, V. Perina, V. Svorcik, V. Rybka, V. Popok, Nucl. Instr. And Meth. B93 (1994) 282-287

(48) L. Torrisi, L. Calcagno, A. M. Foti, Nucl. Instr. And Meth., B32 (1988) 142-144

(49) L. Calcagno, R. Percolla, G. Foti, Nucl. Instr. And Meth., B91 (1994) 426-430

(50) M. Raynaud, C. Reynaud, G. Lecayon, E. Balanzat, Nucl. Instr. And Meth. B32 (1988) 173-176

(51) G. Marletta, S. Pignataro, C. Olieri, Nucl. Instr. and Meth. B39 (1989) 792-795

(52) B. Mohadjeri, J. S. Williams, J. Wong-Leung, Appl. Phys. Lett. 66 (15) 1995, pp.1889-1891

(53) J .R. Kaschny, M. Behar, Nucl. Instr. and Meth., B111 (1996) 51-58

(54) B. Soder, J. Roth, W. Moller, Nucl. Instr. and Meth., B32 (1988) 160-165

A. Delcorte, L. T. Weng, P. Bertrand, Proceeding of the 10th International Workshop on Inelastic Ion Surface Collisions (IISC10), 1994

(55) A. Chapiro, Nucl. Instr. and Meth., B32 (1988) 111-114

(56) L. Calcagno, G. Compagnini, G. Foti, Nucl. Instr. and Meth., B65 (1992) 413-422